P-ISSN: 2304-3075; E-ISSN: 2305-4360
International Journal of Veterinary Science
www.ijvets.com; editor@ijvets.com

Research Article https://doi.org/10.47278/journal.ijvs/2022.220

Morphology and Ultrastructural Characteristics of *Platynosomum fastosum* Kossack, 1910 Adults and Eggs

Babi Kyi Soe[1], Arin Ngamniyom[2], Poom Adisakwattana[3], Somporn Techangamsuwan[4], Panat Anuracpreeda[5], Dwight Bowman[6] and Woraporn Sukhumavasi[7,8*]

[1]The International Graduate Program of Veterinary Science and Technology, Faculty of Veterinary Science, Chulalongkorn University, Bangkok 10330, Thailand
[2]Major Environment, Faculty of Environmental Culture and ECO tourist, Srinakharinwirot University, Bangkok 10100, Thailand
[3]Department of Helminthology, Faculty of Tropical Medicine, Mahidol University, Bangkok 10400, Thailand
[4]Department of Pathology, Faculty of Veterinary Science, Chulalongkorn University, Bangkok 10330, Thailand
[5]Parasitology Research Laboratory, Institute of Molecular Biosciences, Mahidol University, Nakhon Pathom 73170, Thailand
[6]Department of Microbiology and Immunology, College of Veterinary Medicine, Cornell University, Ithaca, NY, USA
[7]Parasitology Unit, Department of Pathology, Faculty of Veterinary Science, Chulalongkorn University, Bangkok 10330, Thailand
[8]Feline Infectious Disease and Health for Excellence Research Unit, Microbial Food Safety and Antimicrobial Resistance Research Unit, Animal Vector-Borne Disease Research Unit, Chulalongkorn University, Bangkok, Thailand
***Corresponding author:** vetkwan@hotmail.com, woraporn.s@chula.ac.th

Article History: 22-737 Received: 27-Oct-22 Revised: 28-Nov-22 Accepted: 30-Nov-22

ABSTRACT

Infection with *Platynosomum fastosum*, a liver fluke of domestic cats, can induce biliary obstruction and has been found to be associated with cholangiocarcinoma. To evaluate any new rational drugs, fundamental knowledges of parasite morphology are crucial but detailed morphology has not yet been investigated. Macroscopic, microscopic, and ultrastructural morphology of *P. fastosum* adult worms and eggs were evaluated. The adult fluke was reddish brown with a tamarind leaf-like body shape, 4.5mm in length and 1.5mm in width. Under scanning electron microscope (SEM), the tegumental surface of *P. fastosum* was spineless and covered with slender villous-like projections. Four types of papillae were found, and all were non-ciliated. *P. fastosum* fluke eggs were dark brown with an operculum and had a smooth eggshell surface with an inconspicuous posterior abopercular knob. From both fecal and bile samples, at least 3 types of eggs were present. The average size (mean±SD) of a typical *P. fastosum* egg was 44.2±1.7µm in length and 31.8±2.2µm in width. Under transmission electron microscope (TEM), tegument syncytium was composed of three layers. The first layer was an outermost trilaminate membrane covered by a glycocalyx. The second layer was tegumental cytoplasm composed of 2 types of tegumental granules, lysosomes, mitochondria and microtrabeculae. The third layer attached to a basal extracellular matrix with numerous basal membrane infoldings. This study revealed the first ultrastructural characteristics of *P. fastosum* adult and egg as a fundamental knowledge to use as basic criteria for assessment of anti-parasitic drug development in the future.

Keywords: *Platynosomum fastosum*, Adult, Egg, Morphology, Scanning Electron Microscopy, Transmission Electron Microscopy, Ultrastructure.

INTRODUCTION

Platynosomum fastosum (synonymous with *Platynosomum illiciens*, *Platynosomum concinnum*), a liver fluke belonging to the family Dicrocoeliidae, is a causal agent of feline platynosomiasis or lizard poisoning which is a neglected hepatobiliary disease in cats. Since this cat liver fluke matures and remains in biliary tracts and gallbladder, it can induce the inflammatory processes depending upon the parasite burden and chronicity. Hence, the infection's outcome can range from asymptomatic to severe and lethal infections. In the case

Cite This Article as: Soe BK, Ngamniyom A, Adisakwattana P, Techangamsuwan S, Anuracpreeda P, Bowman D and Sukhumavasi W, 2023. Morphology and ultrastructural characteristics of *Platynosomum fastosum* Kossack, 1910 adults and eggs. International Journal of Veterinary Science 12(4): 504-521. https://doi.org/10.47278/journal.ijvs/2022.220

of chronic and/or heavy infection, *P. fastosum* can induce mottled liver, gallbladder distension, hepatitis, cholangiohepatitis, cholecystitis, periductal fibrosis, biliary cirrhosis, and biliary obstruction (Basu and Charles 2014; Ramos et al. 2016; Nur-Amalina et al. 2022). Besides, *P. fastosum* infection has been found to be associated with cholangiocarcinoma (Andrade et al. 2012).

Prevalence of *P. fastosum* infection was reported worldwide with ranges between 15 and 85% in both tropical and subtropical regions (Basu and Charles 2014). In Thailand, between the years 2017 and 2020, this parasite seemed to be more commonly recognized and detected than did in previous local reports (Jitsamai et al. 2021). In the year 2020, the prevalence was reported to be 8.9% in Bangkok and vicinities presumably due to increased sampling numbers yielding higher sensitivity of fecal egg detection (Personal communication). Cats can be infected by consuming *P. fastosum* metacercaria-containing prey animals that serve as either the second intermediate or paratenic hosts. Terrestrial lizards have been suspected to play a role in the *P. fastosum* life cycle as a paratenic host that they consume metacercariae-infected terrestrial isopods. The terrestrial isopods receive the sporocyst by ingestion of land snails that previously consumed the environmentally contaminated *P. fastosum* eggs. So far, *Subulina octona* was reported as one of the first intermediate host whereas species of a terrestrial lizard (*Anolis cristatellus*) was reported as a paratenic host (Pinto et al. 2014).

Although praziquantel is recommended as a specific treatment for *P. fastosum* infection in cats, the efficacy of this drug is low, with only 50% efficacy even at a high dose of 20mg/kg, as the adult worms were still present in the cat livers without egg shedding (Lathroum et al. 2018). Whenever a new generation of anti-trematode agent becomes available, dosage titration studies will be required for drug efficacy evaluation. A fundamental knowledge of *P. fastosum* tegument structure is critical to assist in determining the mode of action and drug efficacy analyses. The trematode's tegument is an interface layer that plays a vital role in maintaining the homeostasis of the parasite, for example, nutrient absorption, waste product exchange, osmoregulation, self-protection from host digestive enzymes and immune responses. Therefore, disruption of a functional tegument is likely to have significant effects on the sensory stimuli received by the parasite (Sobhon et al. 2000). Since the tegument releases many of the antigens that can stimulate host immune system, it is considered a primary target for any rational drugs and vaccines (Loukas et al. 2007).

Electron microscopic techniques have been used to elucidate the effect of anthelminthics on tegumental function and stability (Toner et al. 2009; Toner et al. 2010). These techniques can be used to determine the surface topography of the parasite and to investigate the common and unique characteristics among the family (Threadgold 1976). Previous studies on ultrastructural characteristics of the tegument have been conducted with the following trematodes that might be found in the bile ducts of cats: *Paragonimus* spp. (Proctor and Gregory 1974), *Paragonimus westermani* (Lee et al. 1987), *Clonorchis sinensis* (Fujino et al. 1979), *Opisthorchis viverrini* (Apinhasmit et al. 1994), and *Schistosoma japonicum* (Gobert et al., 2003). However, to the authors' knowledge, no such studies have been conducted with both the adult worms and eggs of *P. fastosum*.

The pre-mortem diagnosis of feline platynosomiasis has mainly relied on conventional coprological and microscopic techniques to demonstrate the *P. fastosum* egg in cat fecal samples. Centrifugal sedimentation technique is the method of choice to detect operculated fluke eggs (Willard 2000). However, conventional microscopic examination yielded low sensitivity of detection in cases with light infections due to the nature of intermittent egg shedding by *P. fastosum* (Willard 2000; Shell et al. 2015). According to previous reports, the size of *P. fastosum* egg was 34-50μm in length and 23-35μm in width. The egg was operculated, brown, oval in shape and contain a fully developed miracidium (Basu and Charles 2014). To avoid false positive diagnoses, an experienced microscopic examiner is required to differentiate this egg from other helminth eggs and pseudoparasites. Also, if variable size and shape differences of *P. fastosum* eggs would exist depending upon their maturation and fertilization phases as well as inconsistent egg shedding pattern, the knowledge on these variations should be established in order to achieve the accurate final diagnosis of *P. fastosum* infection.

Consequently, the purposes of this study were to perform a comprehensive approach using a stereomicroscope, a light microscope, a scanning electron microscope (SEM) and a transmission electron microscope (TEM) to reveal the macroscopic morphology, microscopic morphology with and without carmine staining, histological features by hematoxylin and eosin staining and ultrastructural morphology of *P. fastosum* adult worm as well as the structural organization of *P. fastosum* tegument, respectively. Also, the variation in morphology and size of *P. fastosum* eggs was assessed using microscopic examination together with topographic ultrastructural assessment for the first time. This valuable information could provide fundamental knowledge as a basis for anthelminthic drug and vaccine efficacy evaluation that may affect tegumental structures and functions of *P. fastosum* in future anthelminthic studies.

MATERIALS AND METHODS

Ethical Statements

The protocol of this study was approved by the Faculty of Veterinary Science, Animal Care and Use Protocol (VET-ACUP) and Institutional Biosafety Committee (CU-VET-IBC), Chulalongkorn University, Thailand (IACUC No. 2031011 and IBC No. 2031054). All the cats that were recruited to this study had their owners' consent.

Sample Collection, Microscopic Examination and Sample Preservation

Isolation of *P. fastosum* Adult Fluke from the Necropsy of Cat Carcasses

Platynosomum fastosum adult flukes were dissected from the liver and gallbladder of naturally infected cats that were brought for routine post-mortem diagnosis in the Pathology Unit, Faculty of Veterinary Science,

Chulalongkorn University, Thailand. Three *P. fastosum*-infected carcasses were recruited in this study to compare the differences of adult fluke morphology by SEM in which the flukes were collected from partially autolyzed and fresh carcasses. The first and the second *P. fastosum*-infected carcasses were stored in 4°C for 2 and 3 days, respectively, before the necropsy day whereas the third carcass was freshly obtained soon after death. Since the last cat yielded fresh and alive *P. fastosum* adult flukes, its adult worms were selected for detailed tegumental surface study using SEM. During necropsy of these 3 carcasses, sterile normal saline was used to thoroughly flush the biliary tracts and gallbladder. The collected adult flukes were rinsed at least 3 times with 50mL sterile normal saline followed by a quick rinse with distilled water to remove the salt. For unstained adult samples, a randomly selected intact fluke was immediately brought for size measurement using a ruler and for morphology record using a stereomicroscope (OLYMPUS, Japan). To preserve adult fluke samples for carmine staining, the parasite specimens were fixed in 10% formalin for 4 days. For sample preparation for SEM and TEM, adult worms were fixed in 2.5% glutaraldehyde in 0.1M, phosphate buffer, pH 7.2 at 4°C for 2 and 8 days, respectively.

Recovery of *Platynosomum fastosum* Eggs from Cat Fecal and Bile Samples

Platynosomum fastosum infected cats had been previously diagnosed by coprological diagnosis as part of another study. The recovery of *P. fastosum* egg from the fecal samples was conducted as previously described (Jitsamai et al. 2021). Fecal samples were collected per rectum and/or colon with a flushing technique using sterile normal saline followed by a PBS-ethyl acetate centrifugal sedimentation technique and microscopic examination using a light microscope (Olympus, Japan). Images of all *P. fastosum* eggs were recorded for further morphological analysis.

Five of these fecal egg-positive cats were recruited to pursue bile sample collection for another clinical study and for ultrastructural morphology analysis of *P. fastosum* egg. Cats were not allowed to feed and drink for 12hrs before blood collection for blood chemistry and hematology assessment to ensure their safety during sedation and anesthetization. Then, they were sedated with 15μg/kg dexmedetomidine via an intramuscular route and were allowed to rest for 5-10min. After sedation, cats were induced with 4mg/kg propofol intravenously. Before intubation, 0.1mL 2% lidocaine solution was locally dropped at the laryngeal area to prevent the laryngospasm. An endotracheal tube, size 3.5-4.5mm, was intubated with lubricant covering the cuff of endotracheal tube. The tube was related to the ventilator machine and maintained with isoflurane. During the anesthetic process, the heart rates, respiratory rates, indirect blood pressure and oxygen saturation of patient cats were closely monitored. Using ultrasound-guided percutaneous cholecystocentesis (PUC) method performed under the recovery of anesthesia, a total sample of 3-5mL of bile fluid was withdrawn from the gallbladder of each cat using 22G, 1.5inch-needle. A wet bile mount was performed on a glass slide followed by microscopic examination of the eggs with morphological assessment. For the *P. fastosum* egg-containing bile sample preparation for SEM, a collected bile sample was centrifuged at 500xg for 5min at 4°C and the supernatant was discarded to obtain *P. fastosum*-containing bile sediment. To rinse the bile sediment, the sample was then resuspended with phosphate-buffered saline and centrifuged for 10min with repeated steps followed by washing with distilled water. Thereafter, the fluke egg-containing sediment was fixed in 2.5% glutaraldehyde in 0.1M phosphate buffer, pH 7.2 at 4°C for 6 days before SEM processing.

Carmine Staining

Carmine staining was performed according to the method previously described (Marhaba and Haniloo 2018). Briefly, after the fixation of the *P. fastosum* adult parasites in 10% formalin for at least 24hr, they were stained with Semichon's acetic carmine overnight and then destained with 1% HCl for 5min and 70% ethanol for 5min. Then, dehydration was performed with a graded series of ethanol (30, 50, 70, 95, 100% for 10min each and 100% twice), followed by clearing in xylene for 5min and mounting the specimen with permanent medium (Permount, Sigma-Aldrich Co.).

Histological Examination of *P. fastosum* Adult Worm

The formalin-fixed paraffin-embedded (FFPE) adult parasite specimens were prepared as previously described with slight modification (Anuracpreeda et al. 2016). Briefly, the adult worms were fixed in 10% formalin for 24hr, then rinsed with tap water and placed in 70% ethanol for 24hr at room temperature. They were then dehydrated using a graded series of ethanol (70, 80, 95, 100% for 1hr each and twice), cleared in xylene for 1hr, twice and then paraffin impregnated for penetration of the tissues for 1hr, twice using an automatic tissue processor (SAKURA VIP S Jr, Japan). Subsequently, the specimens were embedded in paraffin and sliced to a 3-μm-thick section using a microtome (HESTION ERM3000, Australia), followed by staining with hematoxylin and eosin (H&E) using an automatic staining machine (MYR SS30, Spain) and mounted with a permanent medium (Neo-Mount, Merck, Germany) before microscopic examination.

Scanning Electron Microscopy of *P. fastosum* Adult Worms and Eggs

Necropsy-Derived *P. fastosum* Adult Worms

The 2.5% glutaraldehyde-fixed adult parasite specimens were prepared according to the method previously described (Anuracpreeda et al. 2015). Briefly, the specimens were rinsed twice with phosphate-buffered saline and washed once with distilled water for 10min each. After washing, the specimen was dehydrated with graded series of ethanol (30, 50, 70, 95, 100% for 10min each and 3 rounds for 100%), followed by drying in critical point dryer (Leica model EM CPD300, Austria). The specimens were later mounted on aluminium stubs and coated with gold using sputter coater apparatus (Blazers model SCD 040, Germany), at 15mA for 3min. Finally, the specimens were examined under a scanning electron microscope (JEOL JSM-IT300LV, Japan).

Bile-Derived *P. fastosum* Eggs

A 2.5% glutaraldehyde-fixed fluke egg sediment retrieved from a cat bile sample was further processed for SEM according to previously published protocol (Shin et al. 2009). Cover slip was prepared by cutting into small pieces (size less than $1cm^2$). The specimen was coated with a drop of poly-L-lysine for 10min followed by transferring it onto a cover slip. After 15min, the cover slip was rinsed two times with phosphate-buffer saline and washed once with distilled water (3-5min in each step). After washing, the specimen was dehydrated with graded series of ethanol (concentration of 30, 50, 70, 95, 100% for 10min in each step and 3 rounds for 100%). The specimen was then dried in critical point dryer (Leica model EM CPD300, Austria). After drying, the egg samples were stuck on aluminium stubs using double sided carbon adhesive tape and coated with gold using sputter coater apparatus (Blazers model SCD 040, Germany) at 25mA for 2min. Then, the sample was examined under SEM (JEOL JSM-IT300LV, Japan).

Transmission Electron Microscopy of *P. fastosum* Adult Worms

The 2.5% glutaraldehyde-preserved *P. fastosum* adult samples were prepared according to the protocol described (Anuracpreeda et al. 2016) with slight modification on filtration step. For the washing step, phosphate buffered saline was used to wash 3 times and post-fixed in 1% osmium tetroxide in 0.1M sodium cacodylate buffer, pH 7.2 at 4˚C for 1hr. Thereafter, the specimen was washed in distilled water and subsequently incubated in 0.5% aqueous solution of uranyl acetate, pH 5.0, containing 45mg/mL sucrose, at 4˚C for 20min. Then, the specimen was washed 3 times in distilled water, followed by dehydration in graded series of ethanol 30, 50, 70, 95 and 100%, 10min for each step. Subsequently, the tissue blocks were infiltrated using 1:1 ratio of propylene oxide and resin mixture containing Araldite-502, Dodecenyl Succinic Anhydride (DDSA) and Dimethylaminomethyl-phenol (DMP-30) (EMS, Hatfield, USA) at room temperature overnight. Then, the specimens were transferred to pure Araldite-502 for at least 12hr at room temperature and incubated at 60˚C for 48hr. Thin sections were cut and collected on formvar-coated 300-mesh copper grids. Then, ultrathin sections were stained with uranyl acetate and lead citrate for 30min each. Finally, ultrastructural characteristics of *P. fastosum* was checked using TEM (JEOL JEM, 2100, Japan), operating at 80kV.

RESULTS

Morphology of *P. fastosum* Adult by Macroscopic Examination

At necropsy, several adults *P. fastosum* worms were dissected from the biliary tracts and a gallbladder of a naturally infected cat carcass and placed in 60mm-Petri Dish containing sterile normal saline. The natural color of this worm was reddish brown (Fig. 1A). Based on a ruler placed underneath the Petri Dish, the size of this selected worm was 4.5mm in length and 1.5mm in width. The uterus filled with eggs was dark brown in color beginning two third of the worm's body extending to the posterior end (Fig. 1B).

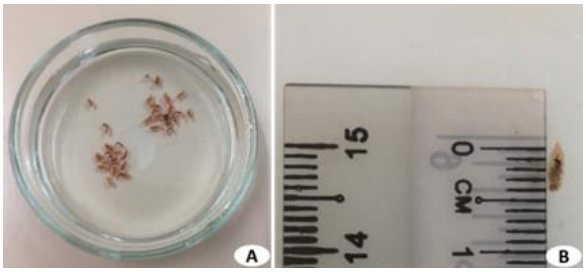

Fig. 1: Morphology of *Platynosomum fastosum* freshly isolated at necropsy of a fresh cat carcass. (A) *P. fastosum* adult flukes dissected from a cat's liver and placed in sterile normal saline in a 60mm Petri Dish. (B) The adult *P. fastosum* can be seen to be about 5mm in length being also translucent and slightly reddish brown.

Morphology of *P. fastosum* Adult by Microscopic Examination

With higher magnification under the stereomicroscope, the *P. fastosum* adults were lanceolate in shape (Fig. 2). The internal organs in the unstained worm were clearly visible (Fig. 2A). Better contrast of certain organs, i.e., testes, ovary and vitelline glands of this worm were clearly demonstrated by carmine staining (Fig. 2B). The bilateral intestinal ceca extending to the terminal end and vitelline ducts were present in unstained worm (Fig. 2A) whereas they were not easily apparent in this carmine-stained worm (Fig. 2B). These two selected worms had a size of 4.4mm in length and 1.2mm in width. The whole body was flat, spineless, and elongated with two prominent suckers, oral and ventral. The anterior end was slightly rounded with the oral sucker and the body was tapered posteriorly. Both oral and ventral suckers were circular in shape. The beginning of the cirrus sac occurred near the bifurcation of the intestinal caeca. Two similar-sized lobular testes were arranged in side-by-side and located in the anterior half of the worm. Below the testes, an oval-shaped ovary was located just to the right of the median vertical axis of the worm. The dark coiled uterus filled with many dark brown eggs occupied two third of the body and extended to the terminal end. Below the common genital pore, the uterus passed through the

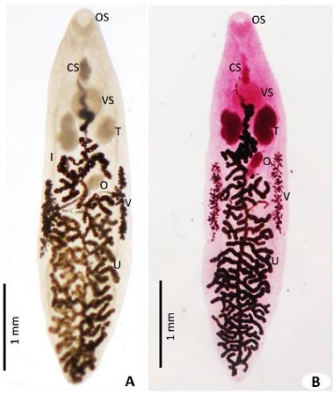

Fig. 2: Adult *Platynosomum fastosum* observed under the stereomicroscope. (A) Fresh and unstained *P. fastosum* adult fluke had a translucent tamarind leaf-like shape. (B) Carmine staining of adult fluke revealed a different contrast and clear visibility of certain organs. Note: oral sucker (OS), cirrus sac (CS), ventral sucker (VS), two testes in side-by-side position (T), intestinal caeca (I), ovary (O), vitelline gland (V) and uterus filled with eggs (U).

median axis between 2 testes. Additionally, numerous vitelline follicles were bilaterally formed into glands at the middle region of the body (Fig. 2A and B).

Characteristics of *P. fastosum* Adult Examined by SEM

Whole Ventral Body

To compare the morphology of the ventral body surface of *P. fastosum* specimens, 3 *P. fastosum* adult flukes were collected from each of the 3 different naturally infected cats by necropsy. The worms in Fig. 3A and 3B were not collected from fresh cat carcasses as the carcasses were kept at 4°C for 2 and 3 days, respectively, prior to necropsy and worm fixation. From the scanning electron micrograph, the body of both worms was relaxed with a protruded cirrus midway between oral sucker and ventral suckers (Fig. 3A and 3B). In contrast, the worm isolated from a recently dead cat and immediately fixed with 2.5% glutaraldehyde seemed to be slightly contracted without a protruded cirrus (Fig. 3C). The general morphology of all 3 flukes was a symmetrical tamarind leaf-like shape and dorsoventrally flattened. The mean body size of these 3 worms (mean±SD) was 4.1±0.21mm in length and 1.2±0.14mm in width. The oral sucker was located in a subterminal position, and the ventral sucker was located about one fourth of the body length from the anterior end. The oral sucker was smaller than the ventral sucker. The opening of oral sucker faced anteroventrally whereas that of ventral sucker faced ventrally. For this freshly preserved fluke (Fig. 3C), the common genital pore without protruded cirrus was located on the midline between the oral and ventral suckers. When the body length of this worm was arbitrarily divided into three regions, anterior, middle, and posterior, the widest part of the body was located around the end of two thirds of the body. Below the widest part, the body is slightly tapering down to posterior end (Fig. 3C).

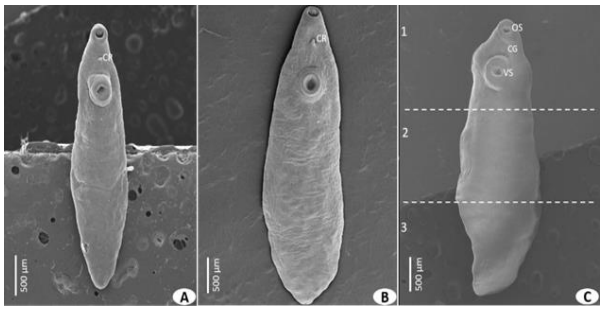

Fig. 3: SEM micrographs of the whole ventral body of 3 *Platynosomum fastosum* adult flukes collected from 3 different infected cats by necropsy. (A and B) Before fixation, both adult worms were not freshly collected from cat carcasses as the carcasses were kept at 4°C for 2 and 3 days, respectively, before the necropsy days. The cirrus (CR) of both worms protruded from the body midway between the oral sucker (OS) and the ventral sucker (VS). (C) The worm was isolated from a recently dead cat and immediately fixed with 2.5% glutaraldehyde at 4°C. The common genital pore (CG) was seen without a protruding cirrus. When the body length of this worm was arbitrarily divided into 3 regions: anterior, 1; middle, 2, and posterior, 3, the widest part of the body was located around two thirds of the body. Note for the image magnification: A, 35x; B and C, 30x.

Oral Sucker and Associated Papillae

From the worm in Fig. 3C, detailed structures were further demonstrated with higher magnification (Fig. 4). The oral sucker of this *P. fastosum* adult fluke was slightly ellipsoidal in shape. The dimension of oral sucker opening was 125µm in horizontal diameter and 75µm in vertical diameter (Fig. 4A). When the apical area of the oral sucker was further enlarged, a number of papillae and pores of gland cells were presented. The tegument at the apical region of the oral sucker showed a wrinkled surface. The papillae were scattered on the apical region (Fig. 4B) and evenly distributed on the perimeter of the oral sucker's aperture (Fig. 4C). In some area between each papilla, pores of gland cells were clustered (Fig. 4B). For the perimeter of the oral sucker's aperture, concentric arrangement of papillae with 8 papillae on each side was somewhat symmetrically demonstrated. Between the lining of these papillae, the corrugated folds and grooves were radially arranged towards the center of the oral sucker opening. These corrugations structurally made the oral sucker discrete from the body tegument. Inside the concave side of oral sucker, a pair of papillae was located on the roof of both sides (Fig. 4C). On the oral sucker, at least 3 types of papillae were demonstrated composed of a plate papilla, a button papilla, and a dome papilla. The plate papilla was flat and associated with cross-linking folds. The size of a plate papilla is >5µm in diameter (Fig. 4D). The button papilla was constructed from extensive binding of tegument folds and immersed their lining inside the tegument depression. The diameter of a button papilla was >5µm (Fig. 4E). The domed papilla protruded from the surface and was surrounded by tegumental folds with a diameter of <10µm (Fig. 4F).

Ventral Sucker and Associated Papillae

The surrounding tegument surface of ventral sucker seemed to protrude with large corrugating structures. The aperture of this ventral sucker was about 175µm in horizontal diameter and about 100µm in vertical diameter. A number of papillae were symmetrically dispersed on both outer and inner rims of the ventral sucker. On the outer rim, 6 papillae were arranged in a hexagonal shape (as shown by a connecting imaginary broken line) with radially arranged folds and grooves (Fig. 5A). Interestingly, another worm collected from the same cat carcass, happened to have a naturally everted ventral sucker making the original internal hollow structure of the concavity become exposed as a smooth dome shape decorated with papillae at its base and its surface. A similar hexagonal arrangement of papillae located on the outer rim of the ventral sucker was also found (Fig. 5B). At the 430x magnification to enhance the square inset in Fig. 5A, circular arrangement of 10 papillae on the inner rim of the ventral sucker are shown (Fig. 5C). At 5,000x magnification to enhance the papillae on the outer and inner rim of the ventral sucker indicated in Fig. 5A with a white arrow and a black arrow, respectively, a dome-shaped papilla on the outer rim seemed to have a couple of crossing folds on the surface with incomplete tegument depression at their base (Fig. 5D), whereas a dome-shaped papilla on the inner rim had a smooth surface (Fig. 5E). The size of these papillae was similar at about 10µm in diameter.

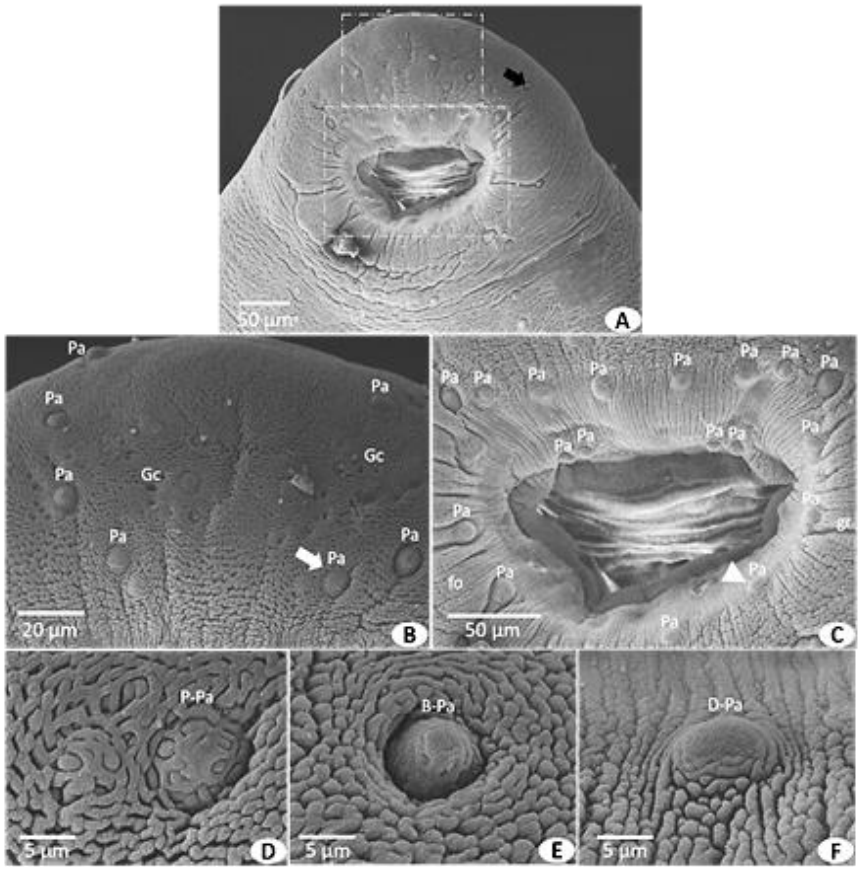

Fig. 4: SEM micrographs of an adult *Platynosomum fastosum* oral sucker and associated papillae. (A) The apical and central areas of the oral sucker are shown and further enlarged in (B) and (C), respectively. (B) On the apical surface of the oral sucker, a number of papillae (Pa) and pores of gland cells (Gc) are present. (C) Concentric arrangement of a number of papillae (Pa) and radial arrangement of folds (fo) and grooves (gr) are on the perimeter of the oral sucker's aperture. (D-F) At least 3 types of papillae were demonstrated composed of a plate papilla (P-Pa), a button papilla (B-Pa) and a dome papilla (D-Pa) in which the papillae indicated with a white arrow, a black arrow, and a white arrowhead in Fig. 4B, Fig. 4A, and Fig. 4C were respectively enlarged. Note for the image magnification: A, 300x; B, 800x; C, 566x (digital zoom); D-F, 5,000x.

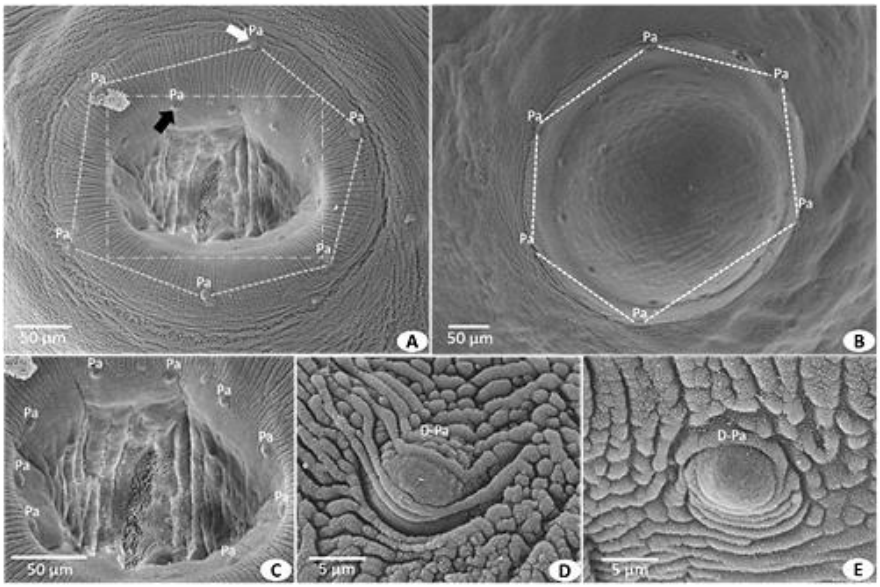

Fig. 5: SEM micrographs of *Platynosomum fastosum* adult fluke's ventral sucker and associated papillae. (A) On the outer rim of the ventral sucker, 6 papillae (Pa) were arranged in hexagonal shape as shown by a connecting broken line. (B) The ventral sucker of another worm, collected from the same cat carcass, happened to be naturally everted making the original internal hollow structure of the concavity appear as a smooth dome shape decorated with papillae at its base and its surface. The similar hexagonal arrangement of papillae (Pa) located on the outer rim of the ventral sucker are also shown through a connecting broken line. (C) Enlargement of the rectangle inset in Fig. 5A, circular arrangement of papillae on the inner rim of the ventral sucker are clearly shown. (D and E) From a white arrow and a black arrow indicated in Fig. 5A, dome-shaped papillae (D-Pa) were shown. Note for the image magnification: A, 300x; B, 250x; C, 430x (digital zoom); D and E, 5,000x.

Cirrus

Between the oral and ventral suckers, the cirrus was extruding on a worm collected from 2 different cat carcasses. From the same worm presented in Fig. 3A (retrieved from a partially autolyzed carcass kept at 4°C for 2 days before necropsy followed by fixation of the worm), the surface of this protruded cirrus revealed an annularly folded structure (Fig. 6A) whereas the cirrus of the worm isolated from a recently dead cat carcass followed by immediate preservation had a reverse funnel shape with a wrinkled surface (Fig. 6B).

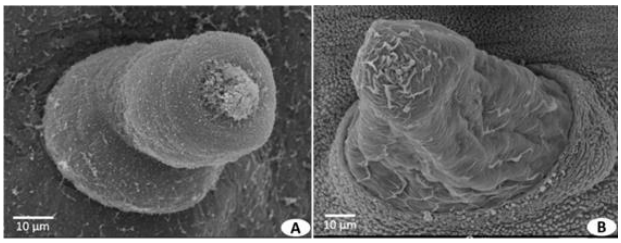

Fig. 6: SEM micrographs of the male reproductive organ, the cirrus, of *Platynosomum fastosum* adult flukes collected from 2 different cat carcasses. (A) From the same worm presented in Fig. 3A, retrieved from a partially autolyzed carcass kept at 4°C for 2 days before necropsy followed by fixation of the worm, the surface of this protruded cirrus revealed an annularly folded structure. (B) From the worm isolated from a recently dead cat carcass followed by immediate preservation, a reverse funnel shape with a wrinkled surface of this cirrus being shown. Note for the image magnification: A, 1,600x and B, 1,200x.

Anteroventral Region of the Worm and Associated Papillae

To demonstrate the tegument and associated papillae in the areas below the oral and below the ventral suckers, images from a rectangle and a square inset from Fig. 7A were further enlarged. Below the oral sucker towards the upper area of the ventral sucker, papillae were bilaterally lined in a vertical row (Fig. 7B). The tegumental surface below a ventral sucker was decorated with the same type of papillae and they were sparsely scattered (Fig. 7C). The papillae found in both regions seemed to be similar in shape. Based on the 2 representative papillae below the ventral sucker area indicated with white arrows in Fig. 7C, these papillae were embedded among tightly dense columnar tegumental projection (Fig. 7D). From the square inset image in Fig. 7D, a rosette cauliflower-shaped papilla was observed with its series of tightly packed tegumental projections and surface outgrowths. The size of this rosette papilla was <5µm in diameter (Fig. 7E).

Ventral and Dorsal Tegument of the Adult Worm

Based on 3 randomly selected ventral tegument shown in inset images (Fig. 8A), the topographical characteristics of anteroventral region was covered with slender villous-like projections that were densely packed (Fig. 8B). For the middle part of the ventral body, a lattice of irregular sized knob-like projections surrounded by shallow furrows made the tegumental surface look knobbly (Fig. 8C). For the posteroventral surface, the short finger-like projections were consistent in size and were densely packed thus the bottom of the furrow was not visible (Fig. 8D). For the tegument of the dorsal side, 3 inset images were also randomly selected for examination of the anterior, middle, and posterior regions (Fig. 8E). For the anterodorsal region, villous-like projections of tegument were formed as transverse bundle or fold alternating with horizontal groove (Fig. 8F). At the middle part of the dorsal tegument, a lattice of irregular size of lumps incorporated with shallow furrows made the surface look lumpy (Fig. 8G). For the posterodorsal section, the short finger-like projections were consistent in size and densely packed thus the bottom of the furrow was not visible (Fig. 8H).

Dorso-Apical and Posterior Terminal End of the Adult Worm

Dorso-apical region showed a few papillae scattered as a single or in groups (Fig. 8I). For this single papilla (arrowhead indicated in I), a dome-shaped papilla was observed (Fig. 8J). A small indentation at the termination of the posterior body was present (Fig. 8K). This was the excretory pore (Ep) exhibiting a hole-like structure (Fig. 8L).

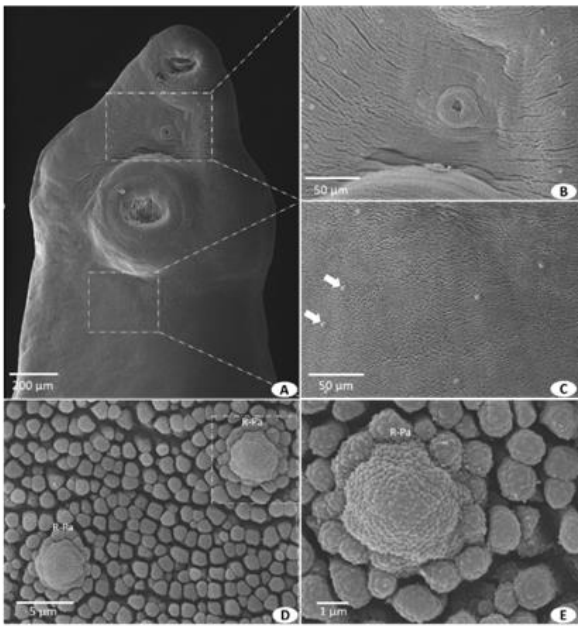

Fig. 7: SEM micrographs of *Platynosomum fastosum* adult fluke's anteroventral region and associated papillae. (A) Rectangle and square inset images of the tegument area between the oral and ventral suckers and the area below ventral sucker were further enlarged in (B) and (C), respectively. (B) Below the oral sucker towards the upper area of the ventral sucker, a row of papillae was arranged in a linear pattern on both sides. (C) The tegumental surface below a ventral sucker was decorated with the same type of papillae being sparsely scattered. (D) Two representative papillae indicated with white arrows in (C) were further enlarged. These papillae were embedded among tightly dense columnar tegumental projections. (E) From the square inset image in (D), a rosette papilla (R-Pa) was classified based on the cauliflower-like outgrowth of the surface. Image magnification: A=80x; B=376x (digital zoom); C=500x; D=5, 000x; E=10,000x.

Morphology of the Bile-Derived *P. fastosum* Eggs from Microscopic Examination

To observe the morphology of *P. fastosum* eggs from the original source where the adult worms shed and deposit their eggs into the gall bladder, PUC was performed to collect the bile from *P. fastosum*-infected

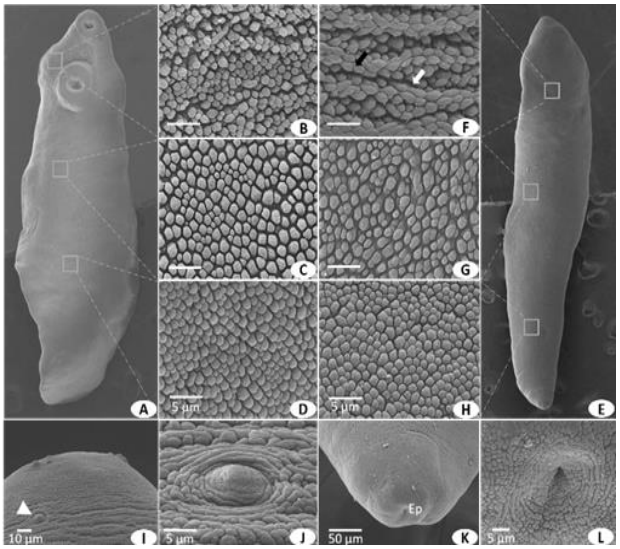

Fig. 8: SEM micrographs of ventral and dorsal tegument as well as dorso-apical and posterior terminal end of adult fluke *Platynosomum fastosum*. (A) For the ventral side, the tegument of the anterior, middle, and posterior regions was randomly selected to be enlarged as indicated inset images. (B) For the tegument of anteroventral region, the different height of slender villous-like projection was found densely packed. (C) A lattice of irregular size of knobs surrounded by shallow furrows made the tegumental surface of the middle part of the ventral body knobbly. (D) For the posteroventral part, the short finger-like projections were consistent in size and were densely packed thus the bottom of the furrow was not able to be seen. (E) For the dorsal side, the anterior, middle, and posterior regions of the tegument were also randomly selected as indicated inset images. (F) For the anterodorsal region, villous-like projections of tegument were formed as transverse bundle or fold (black arrow) alternating with horizontal groove (white arrow). (G) At the middle part of the dorsal tegument, a lattice of irregular size of lumps incorporated with shallow furrows made the surface lumpy. (H) For the posterodorsal part, the short finger-like projections were consistent in size and were densely packed thus the bottom of the furrow was not able to be seen. (I) Dorso-apical region showed a few numbers of papillae scattered as a single or in group. (J) For this single papilla (arrowhead indicated in I), dome-shaped papilla was presented. (K) Indentation at the posterior terminal end was shown. (L) Enlargement of (K), excretory pore (Ep) exhibiting a hole-like structure was clearly present. Image magnification: A and E=30x; B-D and F-G=5000x; I=1000x; J=5000x; K=500x; L=3000x.

cats followed by wet mounts of the bile. Under a light microscope at 40x magnification, the natural dark brown color of unstained *P. fastosum* eggs was clearly discernible (Fig. 9A). At 100x magnification, a varied size of *P. fastosum* eggs was presented (Fig. 9B). Before submission of bile-derived *P. fastosum* eggs for scanning electron microscopy (shown in Fig. 11), eggs washed and then fixed in 2% glutaraldehyde revealed different sizes and color shades of eggs trapped within background bile debris (Fig. 9C). Typical and atypical *P. fastosum* eggs were observed. At 400x magnification, the *P. fastosum* egg was operculated, brown, and elliptical in shape containing well-developed ciliated miracidium in which 2 clusters of germ balls were located on its posterior. Its size was 44µm in length and 32µm in width. An abopercular knob was present on the thick shell opposite to the operculum (Fig. 9D). Apart from the typical form in which most of the structures were clearly visible, *P. fastosum* egg morphology with a long elliptical shape containing undefined miracidium, developing embryos associated vitelline cells, were demonstrated (Fig. 9E). In Fig. 9F, the typical form of *P. fastosum* eggs happened to be located above another form for morphological comparison. The egg in the lower left corner was found to be smaller and lighter in color than did the typical egg. With a distinct operculum and thicker eggshell, this egg had large and scattered germ balls inside the undefined content. In addition to 3 different types of *P. fastosum* egg morphology commonly seen in bile from our study, atypical morphology of *P. fastosum* eggs derived from one cat was also found as smaller in size but with consistent brown color (Fig. 9G-I). Three eggs were subspherical embryonated with one egg having an extended large lobe (Fig. 9G). For the egg in the lower part of Fig. 9H compared to the upper one consistent to the morphology found in Fig. 9F, this egg was asymmetrically oval, small with inconsistent thickness of shell and without discernible content. Interestingly, there was an embryonated egg with morphology similar to conjoined twins with the atypical germ ball inside (Fig. 9I). Variable size differences of *P. fastosum* eggs selected for analysis were shown (Table 1). As a result, the bile eggs were proposed to be classified into three groups: mature, immature and unfertilized eggs (Fig. 9D-F).

Morphology of the Cat Feces-Derived *P. fastosum* Fluke Eggs from Microscopic Examination

To observe the morphology of *P. fastosum* eggs isolated from infected cat fecal samples and to compare with the morphology of *P. fastosum* eggs found in bile, centrifugal sedimentation was performed followed by microscopic examination under a light microscope. At least 3 forms of *P. fastosum* egg were found. Similar to the *P. fastosum* eggs collected from bile sample, the first form was typical as embryonated with a well-developed miracidium, operculated, brown, and elliptical in shape. Two clusters of germ balls were located on its posterior. An abopercular knob was not evidently present and located opposite to the operculum (Fig. 10A). For the 2nd form, operculated and long elliptical in shape containing undefined and granular embryo and possibly germ balls inside the egg were observed (Fig. 10B). For the 3rd form of *P. fastosum* eggs, they were smaller and lighter brown with a distinct operculum and thicker eggshell compared to the typical one. This type of egg had large and scattered germ balls inside the undefined internal content (Fig. 10C). To show the comparative morphology of *P. fastosum* egg with other parasitic stages commonly found in cat feces, we demonstrated some selected fecal samples that happened to have other eggs beside the *P. fastosum* eggs. A partially sporulated *Cystoisospora felis* oocyst and an *Ancylostoma* spp. egg were located next to the *P. fastosum* eggs (Fig. 10D and Fig. 10E, respectively). Importantly, we would like to point out the finding of *Trichuris* spp. egg that was also brown in color and similar in size with *P. fastosum*. However, its barrel shape and bipolar plugs were important characteristics to differentiate *Trichuris* spp. from *P. fastosum* (Fig. 10F).

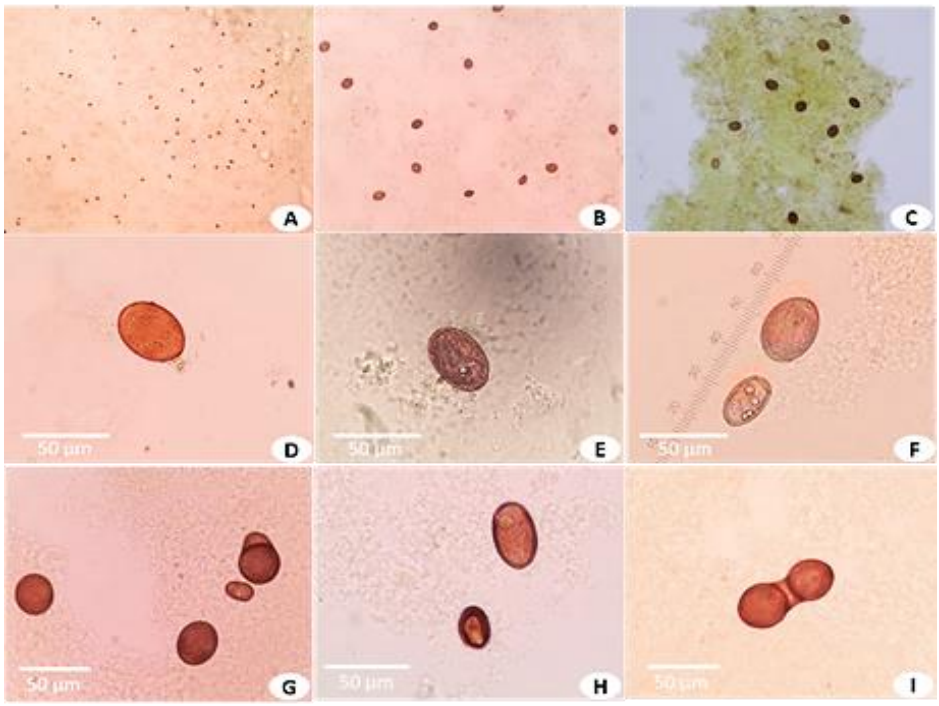

Fig. 9: Morphology of *Platynosomum fastosum* eggs collected from bile samples of infected cats and observed by microscopic examination. (A) The natural dark brown color of *P. fastosum* eggs was discernible at low magnification, 40x. (B) At 100x magnification, a varied size of *P. fastosum* eggs was noted. (C) Before submission of bile-derived *P. fastosum* egg for scanning electron microscopy (shown in Fig. 11), sampling of eggs post sample preparation revealed different sizes and color shade of eggs trapped within bile debris background. (D) A mature *P. fastosum* egg was operculated, brown, and elliptical in shape containing a well-developed miracidium in which 2clusters of germ balls were located on its posterior. An abopercular knob was present on the thick shell opposite the operculum. (E) A *P. fastosum* egg exhibited a long elliptical shape containing undefined miracidium and possibly germ balls inside. (F) A comparison of 2 *P. fastosum* eggs presenting the differences in size and shape. To compare with the mature egg on the top, another type of *P. fastosum* egg was found to be smaller and lighter in color than the mature egg. With a distinct operculum and thicker eggshell, this egg had large and scattered germ balls inside the undefined content. (G-I) Apart from *P. fastosum* egg morphology commonly seen in bile from our study, atypical morphology of *P. fastosum* eggs derived from one cat were also found as smaller in size but with consistent brown color. (G) Three of the eggs were subspherical embryonated with one egg having an extended large lobe. (H) For the lower egg compared to the upper one relevant to the morphology found in (F), this egg was asymmetrically small oval with inconsistent thickness of shell but without discernible content. (I) Morphology similar to conjoined twins of embryonated eggs were found with the atypical germ ball inside. Image magnification: A=40x; B and C=100x.

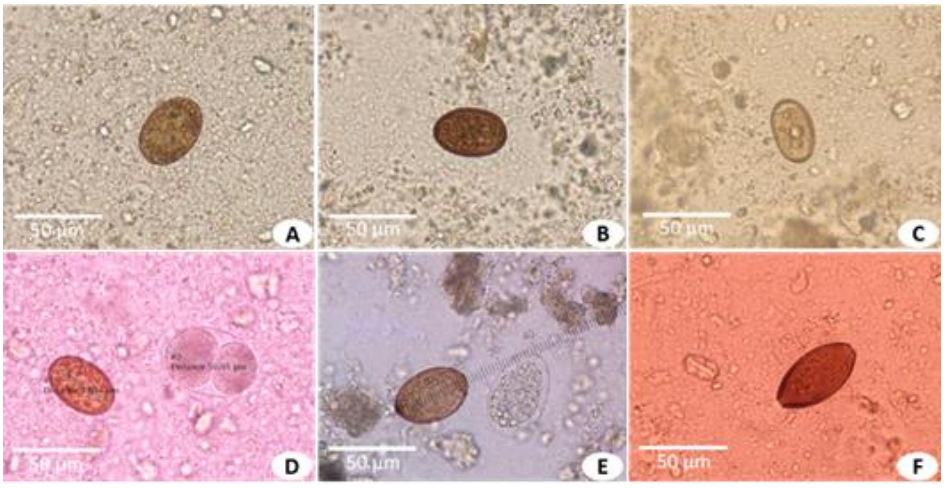

Fig. 10: Morphology of *Platynosomum fastosum* eggs isolated from infected cat fecal samples by centrifugal sedimentation and examined under a light microscope. (A) A mature *P. fastosum* egg was embryonated, operculated, brown, and elliptical in shape. Two clusters of germ balls were located on its posterior. An abopercular knob was evidently not present and located opposite to the operculum. (B) A *P. fastosum* egg was operculated and long elliptical in shape containing undefined and granular embryo and possibly internal germ balls. (C) Another form of *P. fastosum* egg that was smaller, and a lighter brown color was found with a distinct operculum and thicker eggshell compared to the typical one in (A). This egg had large and scattered germ balls inside the undefined internal content. (D) A *P. fastosum* egg was shown beside partially sporulated *Cystoisospora felis* oocyst. (E) A *P. fastosum* fluke egg was shown next to *Ancylostoma* spp. egg. (F) *Trichuris* spp. egg was also brown in color and similar in size to *P. fastosum*, but its barrel shape and bipolar plugs were characteristics that clearly differentiate eggs of *Trichuris* spp. from *P. fastosum*.

Table 1: Measurements of *Platynosomum fastosum* eggs with variable sizes (n=68) in which these eggs were recovered from fecal and bile samples of 14 *P. fastosum* infected cats

Typical/Atypical eggs	Mean±SD (LxW) (µm)
Typical/mature eggs (n=24)	44.2±1.7x31.8±2.2
Dark brown and thick eggshell in elliptical shape, inconspicuous operculum at the anterior end, small knob in the posterior end, fully developed miracidium, bilateral 2 clusters of germ balls	
Atypical/immature eggs (n=21)	43.5±2.0x27.1±2.0
Dark brown and thick shell in long elliptical shape, unremarkable miracidium and germ balls	
Atypical/unfertilized eggs (n=23)	35.3±2.8x23.1±2.4
Lack of embryo and bubbles inside	

Ultrastructural Characteristics of Bile-Derived *P. fastosum* Eggs Using SEM

To observe the ultrastructural features *P. fastosum* egg surface, the egg sample directly taken from a gall bladder of infected cat by PUC shown by microscopic examination (Fig. 9C) was further subjected to SEM. Based on selected SEM micrographs of *P. fastosum* eggs retrieved from bile, the sizes of *P. fastosum* fluke eggs were slightly variable. In Fig. 11A, this egg had an oval shape with the size of 37.5µm in length and 26.2µm in width. The eggshell surface was smooth with inconspicuous operculum at the anterior end. At 6,000x magnification of the same egg, smooth surfaces of the operculum and eggshell were clearly demonstrated but the shoulder rim was not prominent (Fig. 11B). To demonstrate the posterior end of *P. fastosum* egg, an egg with an accidentally broken eggshell was selected to reveal the operculum, shoulder rim and irregular surfaceof abopercular knob at the terminal end (Fig. 11C). At higher magnification, the surface of the eggshell in the terminal region was confirmed to be smooth and the knob was still not very distinct (Fig. 11D). For this smaller sized *P. fastosum* egg, 35µm in length and 25µm in width, an unremarkable operculum, shoulder rim, and abopercular knob were present (Fig. 11E). An enlarged image of an abopercular knob revealed an irregular and slightly pointy surface at the posterior end (Fig. 11F). From the top view of another *P. fastosum* egg, the shape of the operculum was elliptical in shape (Fig. 11G). In Fig. 11H, the lateral view of this *P. fastosum* egg showed an elongated shape like a capsule with an inconspicuous shoulder rim located very close to the apical end. On the surface of this egg, grape-like clusters of cocci bacteria were found in which this was relevant to cholangitis status of this cat based on a culture result.

Tegument of *P. fastosum* Adult Worm by H&E-Stained Histological Examination

To reveal the tegumental surface and partial internal structures of *P. fastosum* adult worms, the formalin-fixed paraffin-embedded adult parasites were prepared, and the cross sections were stained with H&E (Fig. 12A). After observing the parasite tissues at the apical part at 1,000x magnification, a thin layer of the tegument's syncytium was revealed to be without spines. Underneath the reticular lamina layer, parenchyma cells were found in the internal region of the fluke which were connected by loose connective tissues (Fig. 12B). At this magnification, vitelline glands were composed of lobulated vitelline cells (Fig. 12C). The eggshell of *P. fastosum* was thick, brown and operculated. Inside the egg, a miracidium was visible with 2 clusters of germ balls located in the posterior end (Fig. 12D). A cross section of the uterus of the worm showed a number of the contained fluke eggs (Fig. 12E). With enhancement of this image inset, amorphous shape of fluke eggs was present with thick and brown eggshell due to fixation and dehydration artifacts. Based on our finding, the thick brown eggshell nature of *P. fastosum* revealed similar morphology as the eggs from bile and feces as examined microscopically as described above (Fig. 12E and 12F).

Ultrastructural characteristics of *P. fastosum* Adult Worm Using TEM

Layers of the Tegument

To observe the ultrastructural characteristics of the *P. fastosum* adult worms' tegument, samples were fixed, sectioned, and processed for TEM. According to the components of organelles observed across the depth of tegument, tegument of *P. fastosum* can be divided into 3 layers (Fig. 13A). The first layer is the outermost layer with villous-like tegumental projections in which their various lengths were alternately separated by tegument indentations. The exterior tegument surface was covered by trilaminate membrane with a glycocalyx and was devoid of spines (Fig. 13B). Next to the outermost layer, the second layer is tegument cytoplasm which contained tegumental granules, mitochondria and frequently distributed lysosomes as well as micro-trabeculae connecting with the surface syncytium. There were two types of tegumental granules, tegumental granule 1 (TG_1) and tegumental granule 2 (TG_2). TG_1 was spherical in shape with an electron lucent matrix whereas TG_2 were rod-shape having with electron dense matrices. Both TG_1 and TG_2 were densely packed together near the outermost membrane. The tegument cytoplasm appears as a wide area. Due to the presence of microtrabeculae in tegument cytoplasm, it supports internal connections to the tegumental cells (Fig. 13C). The third layer is composed of a basal membrane with infoldings and laying on the basal and reticular laminae. Underneath the tegument syncytium, the areas of basal lamina, reticular laminae, muscle layer and subtegumental layer within tegument cytoplasmic process were enlarged (Fig. 13D). The basal lamina is composed of fibers and slightly stained particles. This layer is connected to the tegument syncytium by means of basal membrane infoldings. The basal lamina appeared to have a trilaminate membrane. Tightly packed filamentous structures were seen in this layer that was intertwined with a translucent gel like substances. This gel-like process connected to basal plasma membrane appears to fill continuously all the space between basal

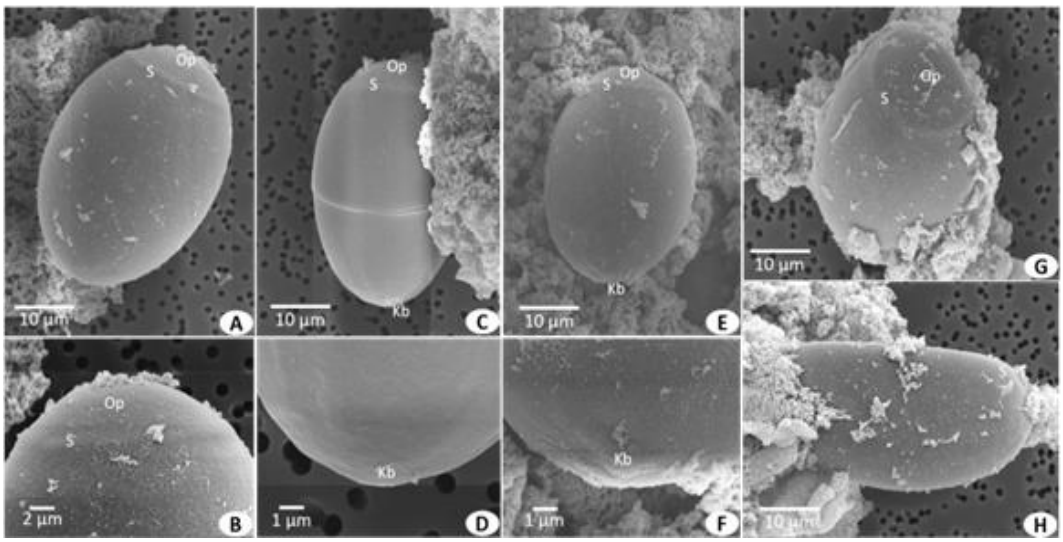

Fig. 11: SEM micrographs of bile-derived *Platynosomum fastosum* eggs directly collected from the gall bladder of infected cats. This sample was the same sample as shown in Fig. 9C for microscopic examination. (A) Inconspicuous operculum (Op) at the anterior end and not prominent shoulder (S) were shown from this tilted orientation of *P. fastosum* egg. (B) Smooth surfaces of the operculum (Op) and eggshell were clearly demonstrated but the shoulder rim (S) was not prominent. (C) With an accidentally broken shell, this *P. fastosum* egg revealed an operculum (Op), shoulder rim (S) and the irregular surface of abopercular knob (Kb) at the terminal end. (D) The surface of the eggshell at the terminal region was smooth and the knob (Kb) was not very distinct. (E) Another *P. fastosum* egg with unremarkable operculum (Op), shoulder rim (S), and abopercular knob (Kb) was present. (F) An enlarged image of an abopercular knob revealed an irregular and slightly pointy surface at the posterior end. (G) From the top view of the *P. fastosum* egg, the shape of the operculum (Op) was elliptical in shape. (H) The lateral view of this *P. fastosum* egg showed an elongated shape with an inconspicuous shoulder rim (S) located very close to the apical end. On the surface of this egg, grape-like clusters of cocci bacteria were found relevant to cholangitis of this cat. Note for the image magnification: Top row (A, C, E, G) and H, 2,500x; Bottom row (B, 6,000x; D and F, 10,000x).

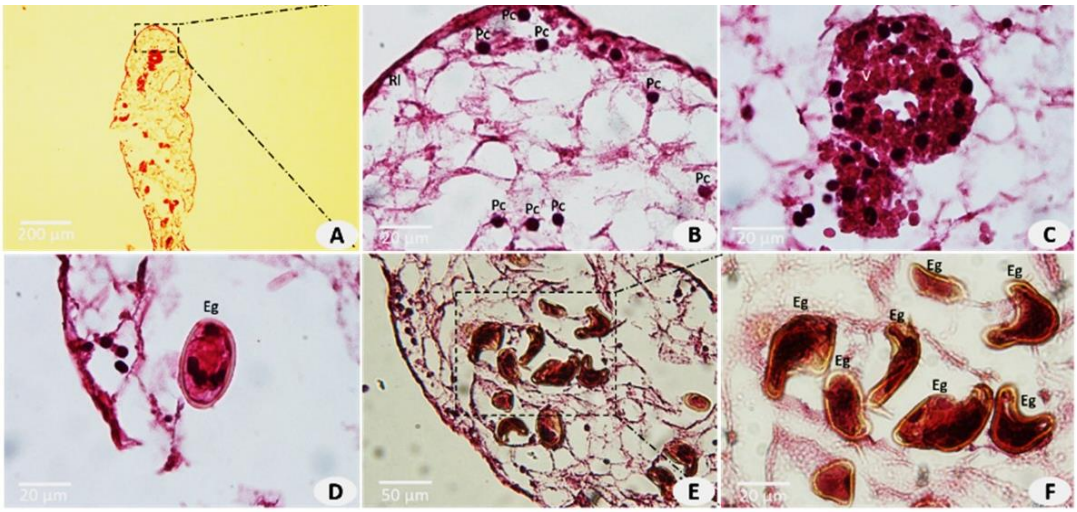

Fig. 12: Histological examination of a *Platynosomum fastosum* adult worm. (A) A cross section of *P. fastosum* adult was further enlarged in Fig. B, C and D. (B) At 1,000x magnification enlarged from the inset image in (A), a thin layer of tegument syncytium was revealed. Underneath the reticular lamina layer (Rl), parenchyma cells (PC) were found in the internal region of the fluke which were connected by loose connective tissues. (C) At 1,000x magnification, vitelline glands (V) were composed of lobulated vitelline cells. (D) The eggshell of *P. fastosum* was thick, brown and operculated. Inside the egg, a miracidium was present with 2 clusters of germ balls located in the posterior end. (E) A cross section of the worm uterus showed a number of fluke eggs inside in which this area was further enlarged in (F). (F) Amorphous shape of fluke eggs (Eg) was present with thick and brown eggshell. Note: H&E staining.

membrane infoldings. Underneath the basal lamina, the reticular lamina was composed of fibers joining the tegument and underlying muscle layers. The lining of basal and reticular laminae was clear and exhibited a fine granular electron lucent matrix (Fig. 13D). The basal and reticular laminae proceed with a narrow channel that runs towards both outer and inner tegument. Under reticular laminae, there were two muscle layers of outer circular and inner longitudinal muscle layer. The subtegumental layer comprised of interstitial fibrous connective tissues. This subtegumental layer also contained limited number of secretory granules and trabeculae-like structures. The secretory granules and trabeculae passed across the granular cytoplasm (Fig. 13D).

Tegumental cells

From the TEM micrographs of areas below the muscle layer of *P. fastosum*'s tegument, the tegumental cell body was present with basic cell structures including distinct nuclear envelope, nucleolus, and cytoplasmic processes (Fig. 14A). From the inset image, it was enlarged to show the components within the cytoplasm of tegumental cell. Both types of tegumental granules (TG_1 and TG_2), secretory granules and Golgi bodies were demonstrated next to the nuclear envelope. Ribosomes, mitochondria, and rough endoplasmic reticulum were also seen. Inside the nucleus, patches of heterochromatin and euchromatin were present (Fig. 14B).

In addition, the tegumental cell processes seem to be packed with microtubules, that are related to the tegumental syncytium by passing through the basal lamina. Moreover, the tegumental cell membrane was connected to nearby parenchymal cells, but their junctions were not clearly observed (Fig. 14A and Fig. 14B).

Sperm Cells and Ova

To observe the reproductive-related organelles and gametes, TEM micrographs of *P. fastosum* adult fluke's oviduct were analyzed. At the edges of Fig. 15A, 2 oocytes were located among several spermatozoa. A number of mitochondria were observed in this area of the oviduct. With the magnification, cross sections and possibly sagittal sections of the congregation of several spermatozoa (Sp) show distinctive sperm heads and sperm tails associated with microtubules. The tail of each spermatozoon showed the presence of cortical microtubules however the pattern of microtubules could not be clearly identified. After syngamy, the section of microtubules can be observed at the peripheral area of fertilized ovum (Fig. 15B).

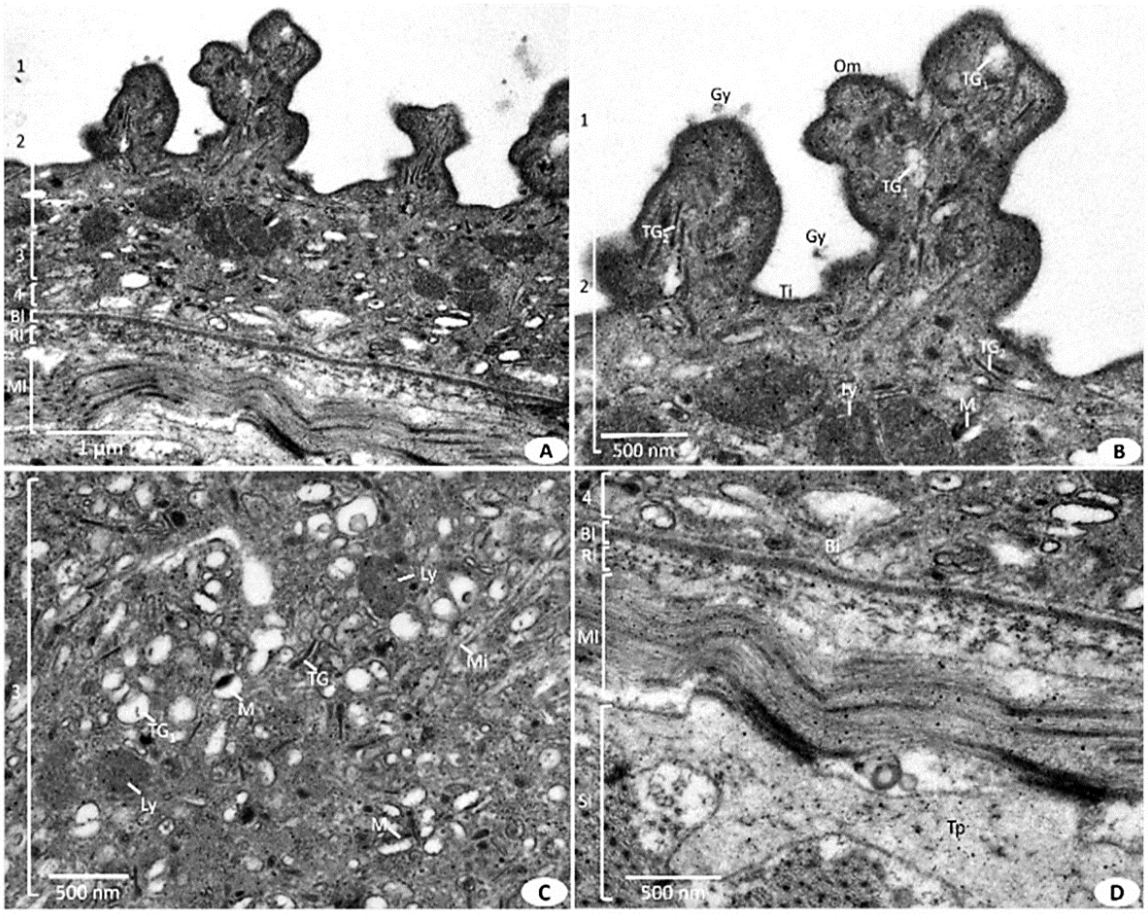

Fig. 13: TEM micrographs of *Platynosomum fastosum* adult fluke's tegument. (A) Cross section of tegument of *P. fastosum* showed 3 layers of tegument syncytium according to the components of organelles; 1, outermost layer; 2, tegument cytoplasm containing tegumental granules and lysosomes; 3, the third layer that lied on basal lamina: basal lamina (Bl); reticular laminae (Rl); and muscle layer (Ml), respectively. (B) In further details of layer 1, tegument outermost layer was covered by outer membrane (Om) with cross section of glycocalyx (Gy). Tegument projections separated by tegument indentation (Ti) were observed in this outermost layer. (C) The second layer is tegumental cytoplasm which contained tegumental granules in which spherical tegumental granule with electron lucent matrix (TG_1) and rod-shape tegumental granule with electron dense matrix (TG_2), mitochondria (M), lysosomes (Ly) and micro-trabeculae (Mi) to connect surface syncytium. (D) The third layer lied on the basal lamina with numerous basal membrane infoldings (Bi) followed by reticular laminae (Rl). Underneath the reticular laminae, the muscle layer (Ml) was followed by subtegumental layer (Sl) within tegument cytoplasmic process (Tp). Note for the magnification of each image: A, 25,000x; B, 51,600x; C, 33,536x and D, 41,735x.

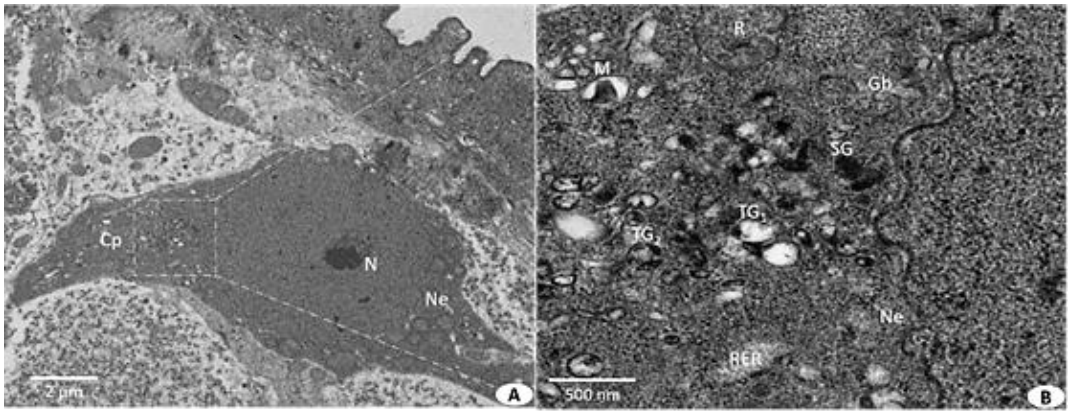

Fig. 14: TEM micrographs of *Platynosomum fastosum* adult fluke's tegumental cell cross section. (A) Under the muscle layer, tegumental cells show distinct nucleolus (N), nuclear envelope (Ne) and cytoplasmic process (Cp). (B) From the inset image in (A), an enlargement of the cytoplasm of tegumental cell, both tegumental granules (TG_1 and TG_2), secretory granules (SG) and Golgi bodies (Gb) are present next to the nuclear envelope (Ne). Ribosome (R), mitochondria (M) and rough endoplasmic reticulum (RER) were also present inside the cytoplasm of the tegumental cell. Note for the image magnification: A, 10,600x and 50,000x.

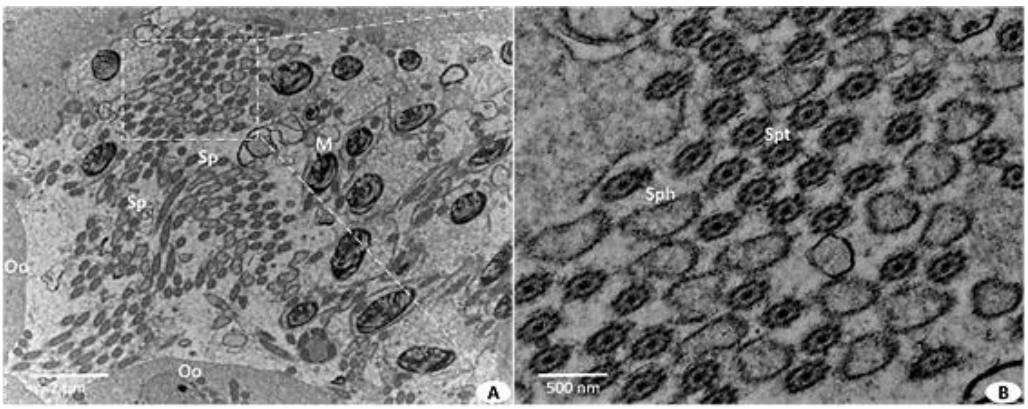

Fig. 15: TEM micrographs of the oviduct of *Platynosomum fastosum* adult fluke. (A) Two oocytes (Oo) were surrounded by spermatozoa (Sp). A number of mitochondria (M) were observed inside the oviduct. (B) With the higher magnification, a cross section of several spermatozoa (Sp) showed distinct sperm heads (Sph) and sperm tails (Spt) associated with microtubules. Note for the magnification of each image: A, 10,000x; B, 50,000x.

DISCUSSION

In this study, we have investigated the morphology of *P. fastosum* adult flukes and eggs by gross examination and with different microscopic techniques. Using the naked eye, the size of this parasite was small, and its color was very similar to liver tissues (Fig. 1). To avoid overlooking this tiny worm, experience and care at necropsy are needed to diagnose this infection at necropsy especially when associated pathology or overt clinical signs are not present. To make the detection of adult *P. fastosum* more vivid and perhaps easy to spot during necropsy, we would like to compare the size of *P. fastosum* with a tamarind leaf which most of veterinarians in tropical countries are familiar with.

When examined by using a stereomicroscope (Fig. 2), the morphology of unstained and stained adult flukes that we investigated were similar to previous reports on morphological description of *P. fastosum* and *P. concinnum*. Based on the description, paired anterior testes and vitellaria on the lateral margins are in line with previously descriptions (Bowman et al. 2002; Basu and Charles 2014). Paired anterior testes are presented in tandem position of *D. dendriticum* (Otranto et al. 2007), whereas two globular posterolateral testes are presented in *Eurytrema coelomaticum* (Leite et al. 2020). In Thailand, two additional genera of liver flukes have been reported in cats (Nimsuphan et al. 2001; Aunpromma et al. 2016) apart from *P. fastosum*, *Opisthorchis viverrini* and *Clonorchis* spp. belonging to the family, Opisthorchiidae. Although the size of these 2 trematodes is also small, the testes of all opisthorchids are located in the posterior part of the body (Enes et al. 2010). Therefore, based on adult worm morphology, we confirmed that the trematode used in this study was identified as *P. fastosum*. Since retrieval of *P. fastosum*-infected cat carcass was challenging at the beginning of our study, we initially obtained 2 partially autolyzed cat carcasses. With the preliminary microscopic examination of the worm morphology, their teguments and internal organs seemed to be intact, so they were subjected to sample preparation for SEM and visualization. At low magnification of SEM, the adult worms looked relaxed with a protruding cirrus (Fig. 3A and Fig. 3B) which may be its actual shape. However, with higher magnification, the tegument and suckers were degenerated (data not shown). We later obtained another carcass in fresh condition, and isolated adult parasites were then subjected to SEM processing. The fresh worms

provided a complete tegument, suckers and papillae, although the body seemed to be slightly contracted and a cirrus of one worm was not protruded (Fig. 3C) or protruded with wrinkled surface (Fig. 6B). To study the ultrastructural features of trematodes, we found that the freshness of sample is critical and cannot be prolonged in the refrigerator longer than one day. Also, to allow the adult worm to be more relaxed, the fixation process should be performed with warm fixative (González et al. 2012).

Based on the previous reports, the location of *P. concinnum* genital pore was at or rather anterior to the branching point of the intestinal ceca (Bowman et al. 2002). This was in line with our results (Fig. 2B and Fig. 3). Also, to observe the location of genital pores with or without cirrus protrusion by the SEM, their locations of all 3 *P. fastosum* worms were in the midpoint between the oral and the ventral suckers (Fig. 3).

On the apical surface of the oral sucker, papillae and pores of gland cells were distributed. Similar to *O. viverrini*, numerous gland cells were found around the oral sucker (Apinhasmit et al. 1993). At least 3 types of papillae composed of plate, button and dome-shaped papillae were seen surrounding the oral sucker. The plate and button papillae seemed to be present on the apical region whereas dome papillae were present on the perimeter of oral sucker's aperture (Fig. 4). To compare these papillae with another worm in the same family, the plate papillae of *P. fastosum* resemble to those of *Dicrocoelium dendriticum* plate papillae which are described as knob like structures, each with a hollow pit surrounded by fine meshwork of tegument ridges (Cifrian and Garcia-Corrales 1988). For the button papillae found on the oral sucker's apical surface of *P. fastosum*, other trematode species also had similar papillae, for example, type C papillae of *Clonorchis sinensis* (Fujino et al. 1979), type B papillae of *Gorgoderina attenuata* (Nadakavukaren and Nollen 1975), and button papillae of *Dicrocoelium dendriticum* (Cifrian and Garcia-Corrales 1988).

P. fastosum's dome papillae on the oral sucker aperture, outer and inner muscular rim of ventral sucker (Fig. 4; Fig. 5), highly resembled those described for *F. hepatica* (Bennett and Threadgold 1975), *Gorgoderina vitelliloba* (Hoole and Mitchell 1981), Paramphistomes (Eduardo 1982) and *D. dendriticum* (Cifrian and Garcia-Corrales 1988). Ciliated papillae were not found in *P. fastosum* whereas a number of such papillae have been reported around oral and ventral sucker of other trematodes, such as *Carmyerius spatiosus* (Anuracpreeda et al. 2015), *Orthocoelium parvipapillatum* (Anuracpreeda et al. 2016), *Fischoederius cobboldi* (Anuracpreeda et al. 2012) and *Opisthorchis viverrini* (Apinhasmit et al. 1993).

Papillae perform various functions depending upon their locations (Hoole and Mitchell 1981). Previously, plate papilla has been shown to be responsible for chemoreceptive functions since this papilla was located around the oral sucker (Otubanjo 1985). Chemoreceptors play essential role for locating hosts and position within hosts since it can perceive chemical compound in their surrounding and responsible for sending this signal as intracellular messages. The button papillae might be involved with contact and mechanoreceptors since this papilla was found at the oral apical portion (Fujino et al. 1979; Hoole and Mitchell 1981). Dome papillae of *P. fastosum* in the present study resemble the conical shape domed papilla of *Gorgoderina vitelliloba* and it could be tangoreceptors to respond to touch and pressure. Since domed papillae were situated on the outer and inner rim of both muscular suckers, this papilla might also serve as stretch receptors. Stretch receptors play critical roles for parasite movement, feeding and attachment (Hoole and Mitchell 1981). The presence of different types of papillae and gland cell pores on the apical region's ventral surface suggested that oral apical placement plays a critical function for nutrient absorption and firm attachment to the host tissue (Apinhasmit et al. 1993).

Due to presence of strong muscular suckers, the worm is able to firmly attach to the biliary epithelial wall. In addition, these suckers could be helpful for nutrient absorption and adaptation of hostile environment since number of papillae are distributed on outer and inner rim of both suckers. Interestingly, there were no spines on entire surface of *P. fastosum*. It has been noted that, suckers are potential targets for anthelmintics drugs (Krupenko 2019), so, we suggest that large muscular suckers of *P. fastosum* could be targeted to interrupt host-parasite mechanism.

The cirrus of *P. fastosum* was annularly folded and had no papillae. This feature is similar to other trematodes of same family such as *D. dendriticum* and *E. coelomaticum*, in which prominent extroversion of a smooth surfaced cirrus has been reported (Cifrian and Garcia-Corrales 1988; Leite et al. 2020). On the contrary, *F. gigantica* has a spinous cirrus dorsally (Dangprasert et al. 2001) and large number of papillae occur around the genital pouch of Paramphistomes (Eduardo 1982). For the new species descriptions of trematode by the light microscopy, the characteristic of cirrus is often used in species identification. However, as far as we know, very little SEM study conducted on the detailed surface description of other trematodes' cirrus.

Rosette papillae of *P. fastosum* were observed below the oral and ventral sucker. These rosette papillae resembled those described in *Dicrocoelium dendriticum* and *Gorgoderina attenuata* (Cifrian and Garcia-Corrales 1988; Mata-López and León-Règagnon 2006) in which these papillae exhibited cauliflower-like structure. Considering their location around ventral midbody, rosette papillae might serve as tangoreceptors (Apinhasmit et al. 1993).

The tegument of *P. fastosum* possess a corrugated surface with slender villous-like projection structure as in *O. viverrini*, in which these projections were said to define a furrowed tegument (Scholz et al. 1992). *F. cobboldi* and *F. gigantica* differ in that they have corrugated transverse folds (Dangprasert et al. 2001; Anuracpreeda et al. 2012). Also, *D. dendriticum* was shown to have an oriented ridge network with tegumental vesicles (Cifrian and Garcia-Corrales 1988). It is possible that the villous-like projections of *P. fastosum* are beneficial to enhance ionic exchange and osmolarity. It might be, as described previously that the arrangement of folds depends upon degree of muscular contraction, thus dorsal anterior region with transverse bundles of corrugated folds alternating

with horizontal grooves appear to be in a highly motile region of the body (Fujino et al. 1979).

In current study, we have investigated variable sizes of *P. fastosum* eggs from both bile and fecal samples. We suggest that the egg with distinct operculum, thick eggshell, large and scattered germ balls inside the undefined content could be unfertilized resembling the unfertilized eggs of *Schistosoma mansoni* (Jurberg et al. 2009). Similar to our study, different morphological features and variable size measurements of *S. mansoni* eggs have been proposed (Cançado et al. 1965). However, only two types of *P. fastosum* eggs have been reported previously, mature eggs with a fully developed miracidium and transparent elliptical shape of immature egg (Palumbo et al. 1976). Our findings of *P. fastosum* egg was in line with the previous study in which the dimension of the egg was 40.61±4.96μm in length and 30.96±5.47μm in width (Ranaraja et al. 2022). Atypical form of *P. fastosum* eggs was seen in the original bile samples, and thus, the microscopic examiner should be aware that they may find typical and atypical *P. fastosum* eggs from fecal sample too, otherwise false negative results may occur. For atypical form of bile-derived *P. fastosum* eggs, the owner informed authors that this cat never received any anthelminthic medication before the day of PUC. So, the cause of eggshell malformation needs to be further explored.

Under SEM, *P. fastosum* eggs are very similar to those of *Eurytrema pancreaticum* (Pinheiro et al. 2015) in shape, size and shell surface smoothness. However, an abopercular knob is not seen in *E. pancreaticum* eggs. In comparison to other minute intestinal fluke eggs, there are thread-like ridges on the eggshell surface of *Pygiodiopsis summa*, multiple minute ridges on *Metagonimus yokogawai* eggshells, rough eggshells on *Heterophyopsis continua*, and a muskmelon-like surface on *C. sinensis* (Lee et al. 2012). A distinct melon pattern is also exhibited on eggshell surface of *O. viverrini* that is thought to play a vital role in attachment of the eggs to aquatic plants to reach their first intermediate host (Apinhasmit et al. 1994).

For H&E staining, the tegument of *P. fastosum* appeared as a thin and homogenous layer with tegument indentations. In contrast with other digenetic trematodes, such as *O. parvipapillatum* and *Paramphistomum gracile*, the teguments exhibited surface folds and grooves (Panyarachun et al. 2013; Anuracpreeda et al. 2016). Cross sections of the uterus showed eggs with thick brown shell as seen in light microscope examinations of bile and fecal samples. Although the fluke was collected from recently dead cat, the fixation in 10% formalin for 48hr may not have been the best fixation to have preserved these structures.

Under TEM, tegumental syncytium of *P. fastosum* can be divided into three layers depending on the components and the depth of the tegument. Tegument indentations occurred along with various tegumental projections. The surface membrane is discontinuously covered with a glycocalyx, and a glycocalyx has been considered to be a typical feature of trematodes, such as *F. hepatica* (Hanna and Trudgett 1983), *F. gigantica* (Sobhon et al. 2000), *O. viverrini* (Apinhasmit et al. 1993), *C. spatiosus* (Anuracpreeda et al. 2015) and *O. parvipapillatum* (Anuracpreeda et al. 2016). As previously described (Threadgold 1976), these glycocalyces were found to be negatively charged with the thought being to protect host immune responses by repelling the attachment of the hosts' immune cells. This negatively charged surface may also serve to gather small molecules, ion particles and amino acids as their nutrient. Herein, we suggest that the glycocalyx might be produced more abundantly by TG_2 granules, since TG_2 granules are consistently dispersed to the outermost membrane and are more likely to be secreted their matrices to tegument surface continuously.

The tegument cytoplasm contained numbers of TG_1 and TG_2 granules, lysosomes, mitochondria and microtubules. Similar to other trematode species, both tegumental granules (TG_1 and TG_2) occurred in *P. fastosum*. The spherical or ovoid (T_0) granules of *F. hepatica* (Hanna 1980) are critical in the juvenile stage to enrich the glycocalyx during parasite migration inside host tissues. When these parasites reach their habitat site, these T_0 granules are totally replaced by similar T_1 granules. However, the number of T_1 granules in adult *F. hepatica* become lesser whereas biconcave or rod shape TG_2 granules are replaced. Likewise, the cytoplasm of the *F. gigantica* tegument contained ovoid granules G_1 and discoid granules G_2. However, G_1 granules are distributed to surface membranes to secrete their contents to contribute to glycocalyx formation (Sobhon et al. 2000). Similarly, in stomach fluke *C. spatiosus*, two types of granules TG_1 and TG_2 occur. However, TG_1 granules were highly dispersed underneath tegument ridges whereas TG_2 granules were distributed through the cytoplasm (Anuracpreeda et al. 2015). As already mentioned, we suggested that the TG_1 granules of *P. fastosum* might be similar to T_1 granules of *F. hepatica*, G_1 granules of *F. gigantica* and TG_1 granules of *C. spatiosus*, whereas TG_2 granules might represent *F. hepatica* T_2 granules, *F. gigantica* G_2 type and *C. spatiosus* TG_2 granules. The rod shaped TG_2 granules of *P. fastosum* are abundantly dispersed near the outermost layer to contribute to the glycocalyx. The secreted tegumental granules appear involved in exchanging materials and replacing of damaged membranes. Lysosomes have been proposed to participate in endocytosis (Anuracpreeda et al. 2016). This layer may serve as storehouse for granules to create new membrane (Sobhon et al. 2000). It has been noted that basal membrane infoldings could be beneficial for enhancement of osmotic and ionic equilibrium (Threadgold 1976). In addition, the tegumental sub-syncytial layer of *P. fastosum* has muscle fibers in which this is similar to other related trematodes such as *C. spatiosus* (Anuracpreeda et al. 2015), *F. gigantica* (Sobhon et al. 2000) and *P. gracile* (Panyarachun et al. 2010). These muscle fibers have been thought to be responsible for parasite movement with strong retraction (Sobhon and Upatham 1990).

According to our findings, only one type of tegumental cell was found in *P. fastosum*. Only one type of tegumental cell synthesized all types of granules in many other digenean species, such as *F. gigantica* (Sobhon et al. 2000), *Bucephalus anguillae* (Filippi et al. 2010), *Lecithochirium musculus* (Filippi et al. 2012), *Deropristis inflata* (Filippi et al. 2013), *O.*

parvipapillatum (Anuracpreeda et al. 2016) and *C. spatiosus* (Anuracpreeda et al. 2015). Conversely, *F. hepatica* showed at least 3 types of tegumental cells (Burden et al. 1983). Both types of tegumental granules (TG_1 and TG_2) are both produced by only one type of tegument cell. Due to presence of microtubules within cytoplasmic process, the granules might be easily transported to the surface tegument (Sobhon and Upatham 1990).

With regard to TEM of reproductive organs, few studies have examined trematode fertilization process and intrauterine eggs. Herein, we have investigated the *P. fastosum* oviduct and spermatozoa. As previously described, microtubules are associated with sperm undulatory movement in which we found them from cross sections of spermatocyte heads and tails (Culioli et al. 2006). Oocytes in the oviduct were found surrounded by spermatocytes. The microtubules in the sperm have been shown to play a critical role in the fusion process of sperm and oocyte (Świderski et al. 2004).

Conclusion

Our study is the first attempt to demonstrate surface topography and ultrastructural characteristics of *P. fastosum*. Understanding basic surface features of both adult worms and eggs could be useful to differentiate between species and might be useful to evaluate the efficacy of any rational drug. Since we observed *P. fastosum* eggs of variable sizes and shapes, the examiner needs to be aware that the misidentification of these poorly formed eggs could lead to the production of a false negative test.

Acknowledgements

The authors would like to thank the staff from STREC lab, Department of Pathology, Faculty of Veterinary Science, Chulalongkorn University and Department of Helminthology, Faculty of Tropical Medicine, Mahidol University for their technical assistance. Moreover, the authors would like to acknowledge the kind support of Dr. Nardtiwa Chaivoravitsakul, Dr. Kongthit Horoongruang, Imaging Unit,and Dr. Siwaporn Pengpis, the Feline Health Center, Small Animal Teaching Hospital, Faculty of Veterinary Science, Chulalongkorn University for the cat physical examination and bile sample collection. The authors would like to appreciate the kind cooperation of Dr. Shin Moe Aoke and Dr. Shane Thiha Soe for the adult fluke collection.

Funding

This study was partially supported by the CU Graduate Thesis Grant, Chulalongkorn University (GCUGR1225642029D No. 029), the Graduate Scholarship Program for ASEAN and NON-ASEAN countries, Chulalongkorn University, for BKS; Chulalongkorn University Research Unit for Feline Infectious Disease and Health for Excellence, Grant of Faculty of Veterinary Science, and Chulalongkorn University Research Unit (GRU 6504931004-1) for WS.

Conflicts of interest

The authors declare that the research was conducted in the absence of any commercial or financial relationships that could be construed as a potential conflict of interest.

Authors' contributions

B.K.S. wrote the main manuscript text and prepared all figures. B.K.S. and W.S. are responsible for conceptualization, research funding acquisition, draft revision and author proof revision. B.K.S., W.S., A.N., P.A., S.T., P.Ad. were responsible for methodology. B.K.S, W.S., A.N., P.A., S.T., P.Ad. took part in investigation. B.K.S, W.S., A.N., P.A. performed formal analysis. D.B. was responsible for draft revision and supervision. W.S., A.N., P.A., S.T., D.B. were involved in original draft editing. W.S. was responsible for publication fee acquisition. All authors have reviewed the manuscript.

REFERENCES

Andrade RL, Dantas AF, Pimentel LA, Galiza GJ, Carvalho FK, Costa VM and Riet-Correa F 2012. *Platynosomum fastosum*-induced cholangiocarcinomas in cats. Veterinary Parasitology 190(1-2): 277-280. https://doi.org/10.1016/j.vetpar.2012.04.015

Anuracpreeda P, Chawengkirttikul R and Sobhon P 2016. Surface histology, topography, and ultrastructure of the tegument of adult *Orthocoelium parvipapillatum* (Stiles & Goldberger, 1910). Parasitology Research 115(7): 2757-2769. https://doi.org/10.1007/s00436-016-5024-3

Anuracpreeda P, Panyarachun B, Ngamniyom A, Tinikul Y, Chotwiwatthanakun C, Poljaroen J and Sobhon P 2012. *Fischoederius cobboldi*: a scanning electron microscopy investigation of surface morphology of adult rumen fluke. Experimental Parasitology 130(4): 400-407. https://doi.org/10.1016/j.exppara.2012.02.001

Anuracpreeda P, Phutong S, Ngamniyom A, Panyarachun B and Sobhon P 2015. Surface topography and ultrastructural architecture of the tegument of adult *Carmyerius spatiosus* Brandes, 1898. Acta Tropica 143: 18-28. https://doi.org/10.1016/j.actatropica.2014.12.003

Apinhasmit W, Sobhon P, Saitongdee P, Menayotin S and Upatham E 1994. *Opisthorchis viverrini*: ultrastructure of the tegument of the first-week juveniles and adult flukes. International Journal for Parasitology 24(5): 613-621. https://doi.org/10.1016/0020-7519(94)90113-9

Apinhasmit W, Sobhon P, Saitongdee P and Upatham ES 1993. *Opisthorchis viverrini*: changes of the tegumental surface in newly excysted juvenile, first-week and adult flukes. International Journal of Parasitology 23(7): 829-839. https://doi.org/10.1016/0020-7519(93)90046-2

Aunpromma S, Kanjampa P, Papirom P, Tangkawattana S, Tangkawattana P, Tesana S, Boonmars T, Suwannatrai A, Uopsai S and Sukon P 2016. Prevlence and risk factors for *Opisthorchis viverrini* infection among cats and dogs in six districts surrounding the Ubolratana dam, an endemic area for human Opisthorchiasis in Northeastern Thailand. Southeast Asian Journal of Tropical Medicine and Public Health 47(6): 1153-1159.

Basu AK and Charles RA 2014. A review of the cat liver fluke *Platynosomum fastosum* Kossack, 1910 (Trematoda: Dicrocoeliidae). Veterinary Parasitology 200(1-2): 1-7. https://doi.org/10.1016/j.vetpar.2013.12.016

Bennett C and Threadgold L 1975. *Fasciola hepatica*: development of tegument during migration in mouse. Experimental Parasitology 38(1): 38-55. https://doi.org/10.1016/0014-4894(75)90036-3

Bowman DD, Hendrix CM, Lindsay DS and Barr SC 2002. Feline Clinical Parasitology. Vol 206. In: Wiley Online Library.

Cançado JR, da Cunha AS, de Carvalho DG and Cambraia JS 1965. Evaluation of the treatment of human *Schistosoma mansoni* infection by the quantitative oogram technique. Bulletin of the World Health Organization 33(4): 557.

Cifrian B and Garcia-Corrales P 1988. Scanning electron microscopy of adult *Dicrocoelium dendriticum*. Parasitology Research 74(3): 235-242.

Culioli J-L, Foata J, Mori C and Marchand B 2006. Spermiogenesis and sperm in *Mesostoma viaregginum* (Plathelminthes, Rhabdocoela): an ultrastructural study to infer sperm orientation. Zoomorphology 125(1): 47-56. http://:doi/10.1007/s00435-006-0014-0

Dangprasert T, Khawsuk W, Meepool A, Wanichanon C, Viyanant V, Upatham E, Wongratanacheevin S and Sobhon P 2001. *Fasciola gigantica*: surface topography of the adult tegument. Journal of Helminthology 75(1): 43. https://doi.org/10.1079/JOH200041

Eduardo S 1982. The taxonomy of the family Paramphistomidae Fischoeder, 1901 with special reference to the morphology of species occurring in ruminants. I. General considerations. Systematic Parasitology 4(1): 7-57.

Enes JE, Wages AJ, Malone JB and Tesana S 2010. Prevalence of *Opisthorchis viverrini* infection in the canine and feline hosts in three villages, Khon Kaen Province, northeastern Thailand. The Southeast Asian Journal of Tropical Medicine and Public Health 41(1): 36.

Filippi J-J, Quilichini Y, Foata J and Marchand B 2010. Topography and ultrastructure of the tegument of *Bucephalus anguillae* (Digenea: Bucephalidae), a parasite of the European eel *Anguilla anguilla* (Osteichthyen: Anguillidae). Journal of Parasitology 96(6): 1102-1111. https://doi.org/10.1645/ge-2498.1

Filippi J-J, Quilichini Y and Marchand B 2013. Topography and ultrastructure of the tegument of *Deropristis inflata* Molin, 1859 (Digenea: Deropristidae), a parasite of the European eel *Anguilla anguilla* (Osteichthyes: Anguillidae). Parasitology Research 112(2): 517-528. https://doi.org/10.1007/s00436-012-3162-9

Filippi JJ, Quilichini Y, Foata J and Marchand B 2012. Topography and ultrastructure of the tegument of *Lecithochirium musculus* (Digenea: Hemiuridae), a parasite of the European eel *Anguilla anguilla* (Osteichthyes: Anguillidae). Journal of Morphology 273(4): 361-370. https://doi.org/10.1002/jmor.11032

Fujino T, Ishii Y and Choi DW 1979. Surface ultrastructure of the tegument of *Clonorchis sinensis* newly excysted juveniles and adult worms. The Journal of Parasitology 579-590. https://doi.org/10.2307/3280325

Gobert GN, Stenzel DJ, McManus DP and Jones MK 2003. The ultrastructural architecture of the adult *Schistosoma japonicum* tegument. International Journal for Parasitology 33(14): 1561-1575. https://doi.org/10.1016/s0020-7519(03)00255-8

González CE, Hamann MI and Salgad C 2012. Study of helminth parasites of amphibians by Scanning Electron Microscopy. In: Scanning Electron Microscopy. InTechOpen.

Hanna R and Trudgett A 1983. *Fasciola hepatica*: development of monoclonal antibodies and their use to characterize a glycocalyx antigen in migrating flukes. Parasite Immunology 5(4): 409-425. https://doi.org/10.1111/j.1365-3024.1983.tb00756.x

Hanna REB 1980. Fasciola hepatica: An immunofluorescent study of antigenic changes in the tegument during development in the rat and the sheep. Experimental Parasitology 50(2): 155-170. https://doi.org/10.1016/0014-4894(80)90017-X

Heckmann R, Halajian A, Atif E-N and Wilmien L-P 2014. A Histopathology Study of Caspian Seal (*Pusa caspica*)(Phocidae, Mammalia) Liver Infected with Trematode, *Pseudamphistomum truncatum* (Rudolphi, 1819)(Opisthorchidae, Trematoda). Iranian Journal of Parasitology 9(2): 266.

Hoole D and Mitchell J 1981. Ultrastructural observations on the sensory papillae of juvenile and adult *Gorgoderina vitelliloba* (Trematoda: Gorgoderidae). International Journal for Parasitology 11(5): 411-417. https://doi.org/10.1016/0020-7519(81)90014-X

Jitsamai W, Khrutkham N, Hunprasit V, Chandrashekar R, Bowman D and Sukhumavasi W 2021. Prevalence of endoparasitic and viral infections in client-owned cats in metropolitan Bangkok, Thailand, and the risk factors associated with feline hookworm infections. Veterinary Parasitology: Regional Studies and Reports 100584. https://doi.org/10.1016/j.vprsr.2021.100584

Jurberg AD, Gonçalves T, Costa TA, de Mattos ACA, Pascarelli BM, de Manso PPA, Ribeiro-Alves M, Pelajo-Machado M, Peralta JM and Coelho PMZ 2009. The embryonic development of *Schistosoma mansoni* eggs: proposal for a new staging system. Development Genes and Evolution 219(5): 219. https://doi.org/10.1007/s00427-009-0285-9

Krupenko D 2019. Oral sucker in Digenea: structure and muscular arrangement. Zoomorphology 138(1): 29-37. https://link.springer.com/article/10.1007/s00435-018-0423-x https://link.springer.com/article/10.1007/s00435-018-0423-x

Lathroum CN, Shell L, Neuville K and Ketzis JK 2018. Efficacy of Praziquantel in the Treatment of *Platynosomum fastosum* in Cats with Natural Infections. Veterinary Sciences 5(2): 35. https://doi.org/10.3390/vetsci5020035

Lee J-J, Jung B-K, Lim H, Lee MY, Choi S-Y, Shin E-H and Chai J-Y 2012. Comparative morphology of minute intestinal fluke eggs that can occur in human stools in the republic of Korea. The Korean Journal of Parasitology 50(3): 207. https://doi.org/10.3347/kjp.2012.50.3.207

Lee SH, Park HJ, Hong SJ, Chai JY and Hong ST 1987. In vitro effect of praziquantel on *Paragonimus westermani* by light and scanning electron microscopic observation. Korean Journal of Parasitology 25(1): 24-36.

Leite K, Lopes-Torres E, Souza J, Neves R, Gomes D and Machado-Silva J 2020. *Eurytrema coelomaticum*: updated morphology of adult worms using advanced microscopy experiments. Journal of Helminthology 94. https://doi.org/10.1017/S0022149X19001135

Loukas A, Tran M and Pearson MS 2007. Schistosome membrane proteins as vaccines. International Journal for Parasitology 37(3-4): 257-263. https://doi.org/10.1016/j.ijpara.2006.12.001

Marhaba Z and Haniloo A 2018. Staining of Parasitic Helminths by Extracts of *Allium cepa*, *Juglans regia*, and *Rubia tinctorum*: An Approach to Herbal Dyes. Iranian Journal of Parasitology 13(2): 293.

Mata-López R and León-Règagnon V 2006. Comparative study of the tegumental surface of several species of *Gorgoderina* Looss, 1902 (Digenea: Gorgoderidae), as revealed by scanning electron microscopy. Comparative Parasitology 73(1): 24-34.

Nadakavukaren MJ and Nollen PM 1975. A scanning electron microscopic investigation of the outer surfaces of *Gorgoderina attenuata*. International Journal for Parasitology 5(6): 591-595. https://doi.org/10.1007%2Fs12639-015-0745-2

Nimsuphan B, Prihirunkij K, Pinyopanuwat N and Chimnoi W 2001. Case report: mixed infection of *Platynosomum fastosum* and *Clonorchis sinensis* in cat. Warasan Sattawaphaet https://doi.org/10.3347%2Fkjp.2010.48.2.157

Nur-Amalina N, Watanabe M, Mazlina M, Che-Amat A and Nor-Azlina AA 2022. Feline platynosomiasis in Klang Valley, Malaysia: Diagnosis, pathology and management. Tropical Biomedicine 39(1): 26-35. https://doi.org/10.47665/tb.39.1.006

Otranto D, Rehbein S, Weigl S, Cantacessi C, Parisi A, Lia RP and Olson PD 2007. Morphological and molecular differentiation between *Dicrocoelium dendriticum* (Rudolphi, 1819) and *Dicrocoelium chinensis* (Sudarikov and Ryjikov, 1951) tang and tang, 1978 (Platyhelminthes: Digenea). Acta Tropica 104(2-3): 91-98. https://doi.org/10.1016/j.actatropica.2007.07.008

Otubanjo OA 1985. Scanning electron microscopic studies of the body surface and external genitalia of a dicrocoeliid trematode, *Concinnum epomopis* Sandground 1973. Zeitschrift für Parasitenkunde 71(4): 495-504.

Palumbo N, Taylor D and Perri S 1976. Evaluation of fecal technics for the diagnosis of cat liver fluke infection. Laboratory Animal Science 26(3): 490-493.

Panyarachun B, Ngamniyom A, Sobhon P and Anuracpreeda P 2013. Morphology and histology of the adult *Paramphistomum gracile* Fischoeder, 1901. Journal of Veterinary Science 14(4): 425. https://doi.org/10.4142%2Fjvs.2013.14.4.425

Panyarachun B, Sobhon P, Tinikul Y, Chotwiwatthanakun C, Anupunpisit V and Anuracpreeda P 2010. *Paramphistomum cervi*: surface topography of the tegument of adult fluke. Experimental Parasitology 125(2): 95-99. https://doi.org/10.1016/j.exppara.2009.12.020

Pinheiro J, Franco-Acuña D, Oliveira-Menezes A, Brandolini S, Adnet F, Torres EL, Miranda F, De Souza W and Damatta R 2015. Additional study of the morphology of eggs and miracidia of *Eurytrema coelomaticum* (Trematoda). Helminthologia 52(3): 244. http://doi.org/10.1515/helmin-2015-0039

Pinto HA, Mati VL and de Melo AL 2014. New insights into the life cycle of *Platynosomum* (Trematoda: Dicrocoeliidae). Parasitology Research 113(7): 2701-2707. http://doi.org/10.1007/s00436-014-3926-5

Proctor E and Gregory M 1974. An ultrastructural study of ova of *Paragonimus* species from human and cat faeces. South African Medical Journal 48(46): 1947-1948.

Ramos RA, Lima VF, Monteiro MF, Santana Mde A, Lepold R, Faustino MA, Rinaldi L, Cringoli G and Alves LC 2016. New insights into diagnosis of *Platynosomum fastosum* (Trematoda: Dicrocoeliidae) in cats. Parasitology Research 115(2): 479-482. http://doi.org/10.1007/s00436-015-4763-x

Ranaraja DMAE, Mahakapuge TAN, Thilakarathne DS, Dharmasuriya JYC and Rajapakse RPVJ 2022. Hepatic trematode *Platynosomum* sp. (Dicrocoeliidae) from a domestic cat in Colombo, Sri Lanka: Case report and molecular identification. Veterinary Parasitology: Regional Studies and Reports 34: 100762. https://doi.org/10.1016/j.vprsr.2022.100762

Scholz T, Ditrich O and Giboda M 1992. Study on the surface morphology of the developmental stages of the liver fluke, *Opisthorchis viverrini* (Trematoda: Opisthorchiidae). Annales de Parasitologie Humaine et Comparée 67(3): 82-90. https://doi.org/10.1051/parasite/199267382

Shell L, Ketzis J, Hall R, Rawlins G and du Plessis W 2015. Praziquantel treatment for *Platynosomum* species infection of a domestic cat on St Kitts, West Indies. Journal of Feline Medicine and Surgery 1(1): 2055116915589834. https://doi.org/10.1177/2055116915589834

Shin DH, Lim D-S, Choi K-J, Oh CS, Kim MJ, Lee IS, Kim SB, Shin JE, Bok GD and Chai JY 2009. Scanning electron microscope study of ancient parasite eggs recovered from Korean mummies of the Joseon Dynasty. Journal of Parasitology 95(1): 137-145. https://doi.org/10.1645/ge-1588.1

Sobhon P, Dangprasert T, Chuanchaiyakul S, Meepool A, Khawsuk W, Wanichanon C, Viyanant V and Upatham E 2000. *Fasciola gigantica*: ultrastructure of the adult tegument. Science Asia 26: 137-148.

Sobhon P and Upatham ES 1990. Snail hosts, life-cycle, and tegumental structure of oriental schistosomes. UNDP/World bank/WHO. Special programme for research and training in tropical diseases.

Świderski Z, Conn DB, Miquel J and Młocicki D 2004. Fertilization in the cestode *Gallegoides arfaai* (Mobedi et Ghadirian, 1977) Tenora et Mas-Coma, 1978 (Cyclophyllidea, Anoplocephalidae). Acta Parasitology 49: 108-115.

Threadgold L 1976. *Fasciola hepatica*: ultrastructure and histochemistry of the glycocalyx of the tegument. Experimental Parasitology 39(1): 119-134. https://doi.org/10.1016/0014-4894(76)90019-9

Toner E, Brennan G, McConvery F, Meaney M and Fairweather I 2010. A transmission electron microscope study on the route of entry of triclabendazole into the liver fluke, *Fasciola hepatica*. Parasitology 137(5): 855-870. https://doi.org/10.1017/S0031182009991247

Toner E, McConvery F, Brennan G, Meaney M and Fairweather I 2009. A scanning electron microscope study on the route of entry of triclabendazole into the liver fluke, *Fasciola hepatica*. Parasitology 136(5): 523-535. https://doi.org/10.1017/s0031182009005642

Willard MD and Fossum TW, 2000. Diseases of the gallbladder and extra-hepatic biliary system. In: Ettinger, S.J., Feldman, E.C. (Eds.), Textbook of Veterinary Internal Medicine, 5th Ed. WB Saunders, Philadelphia, USA, pp: 1343.